

Reactive mercury in the troposphere: Model formation and results for Florida, the northeastern United States, and the Atlantic Ocean

Sanford Sillman,¹ Frank J. Marsik,¹ Khalid I. Al-Wali,¹ Gerald J. Keeler,¹
and Matthew S. Landis²

Received 7 November 2006; revised 22 June 2007; accepted 13 August 2007; published 11 December 2007.

[1] We describe the development of a model for transport and photochemistry of atmospheric mercury at the regional scale, along with an application to the eastern United States and adjacent Atlantic Ocean and Gulf of Mexico, and comparison with aircraft-based measurements in Florida. The model is the Community Multiscale Air Quality model (CMAQ) with modifications to include an integrated solution for gas phase and aqueous photochemistry. The expanded chemistry includes O₃, NO_x, organics, sulfur, halogens and mercury. Divalent reactive gaseous mercury (RGM) is formed slowly through gas phase reactions and removed rapidly by aqueous reactions in cloud water. Model results show that elevated RGM (up to 260 pg m⁻³) forms intermittently over the Atlantic Ocean in air masses that have a cloud-free history. Aircraft measurements in Florida show RGM varying between 10 and 250 pg m⁻³ and increasing with altitude, a pattern that is consistent with model results. Ambient RGM would increase by 50% if aqueous reduction reactions were omitted. The model predicts that ambient elemental mercury and RGM anticorrelate in regions where RGM is produced photochemically and correlate in regions dominated by direct emissions. Model results also suggest positive correlations between RGM and SO₂, reactive nitrogen and H₂O₂, which may be used to identify photochemically produced versus directly emitted RGM. RGM in the model is strongly correlated with O₃ during pollution events, and ozone formation from anthropogenic precursors is predicted to cause a significant increase in RGM.

Citation: Sillman, S., F. J. Marsik, K. I. Al-Wali, G. J. Keeler, and M. S. Landis (2007), Reactive mercury in the troposphere: Model formation and results for Florida, the northeastern United States, and the Atlantic Ocean, *J. Geophys. Res.*, 112, D23305, doi:10.1029/2006JD008227.

1. Introduction

[2] Reliably modeling the transport, transformation, and deposition of atmospheric mercury and elucidating the relative importance of local, regional, and global emission sources is currently limited because of, among other things, uncertainties in its atmospheric chemistry. Mercury in the atmosphere is dominated (~98%) by elemental gaseous mercury (Hg⁰) [Schroeder and Munthe, 1998]. Hg⁰ is relatively insoluble in water and unreactive, and its atmospheric lifetime (>30 d) allows for global-scale transport. Divalent reactive gaseous mercury (RGM) in the atmosphere is water-soluble and is efficiently removed through both wet and dry deposition processes. Elevated levels of RGM are typically associated with direct emissions from localized anthropogenic sources, but can also be produced by photochemical conversion from Hg⁰. It is often uncertain whether deposition of mercury is due primarily to local

emission of RGM or to photochemical conversion of transported Hg⁰. In the United States the National Mercury Deposition Network has found the highest rates of mercury deposition in regional background locations have occurred in the southeast (especially Florida), although the highest rates of U.S. mercury emissions are in the northeast and midwest regions in recent years (National Atmospheric Deposition Program, Mercury Deposition Network, available at <http://nadp.sws.uiuc.edu/mdn/>).

[3] Ambient gaseous mercury species are affected by gas phase and aqueous photochemical reactions that involve a wide range of species (O₃, OH, Cl, Br and sulfates). Modeling the transport and transformation of mercury in the atmosphere is a challenge because it involves processes on widely different spatial and temporal scales. Deposition of mercury is affected by localized convective events, and processing by small-scale convective clouds can also affect photochemistry. Photochemical conversion from Hg⁰ to RGM also results in the formation of particulate mercury Hg (p), which frequently occurs as part of multispecies conglomerates. Because deposited mercury can be reemitted from terrestrial and aquatic ecosystems, a complete representation of mercury in the atmosphere should also include surface flux processes as well.

¹Department of Atmospheric, Oceanic and Space Sciences, University of Michigan, Ann Arbor, Michigan, USA.

²Office of Research and Development, U.S. Environmental Protection Agency, Research Triangle Park, North Carolina, USA.

[4] Regional and global-scale models for reactive mercury have been developed by *Pai et al.* [1997], *Shia et al.* [1999], *Xu et al.* [2000a, 2000b] *Petersen et al.* [2001], *Bullock and Brehme* [2002], *Dastoor and Larocque* [2004], *Seigneur et al.* [2004], *Gbor et al.* [2006, 2007], and *Hedgecock et al.* [2005, 2006], and *Selin et al.* [2007]. Model methods were also discussed by *Ryaboshapko et al.* [2002]. These models all use approximate methods for determining concentrations of OH, HO₂ and O₂⁻ in the aqueous phase. For example, *Bullock and Brehme* [2002] and *Gbor et al.* [2006] both use operator splitting with separate calculations for gas phase and aqueous chemistry, so that calculated gas phase OH and HO₂ provide input for the aqueous phase calculation. These methods are an incomplete solution for the aqueous radicals because the latter are short-lived and are influenced by gas-aqueous transport on very short timescales (<100 s). Interactions between gas and aqueous phase photochemistry can lead to decreases in gas phase OH and HO₂ of 70% or more [*Monod and Carlier*, 1999; *Jacob*, 2000].

[5] Here, we present results from a model for regional-scale atmospheric transport and chemistry gas phase mercury and related species. The model is a version of the Community Multiscale Air Quality model (CMAQ) [*Byun and Schere*, 2006] that has been modified to include a simultaneous solution for gas phase and aqueous photochemistry. The modified chemistry represents a departure from the model developed by *Bullock and Brehme* [2002], which also used the CMAQ platform. Particulate mercury and soil recycling have not been included.

[6] We also describe a model application for 15 d in June 2000, for a domain that includes the eastern United States, the Gulf of Mexico and large parts of the Atlantic Ocean. This time period coincides with aircraft-based field measurements of Hg⁰, RGM, and Hg (p) in south Florida that were performed by the U.S. Environmental Protection Agency's National Exposure Assessment Laboratory. Some results from the field campaign are shown in comparison with model results.

[7] We have also used the model to predict correlations between RGM and various other species, including Hg⁰, SO₂, H₂O₂ and O₃. These correlations are important because they are linked to different formation processes for RGM (e.g., direct emission, photochemical production). The predicted correlations may provide a basis for evaluating the importance of atmospheric processes that affect RGM based on ambient measurements.

2. Methods

2.1. Model

[8] The Community Multiscale Air Quality model (CMAQ) [*Byun and Schere*, 2006] has been widely used to investigate urban and regional-scale atmospheric transport and chemistry for gas phase and aerosol species [e.g., *Mebust et al.*, 2003; *Mao and Talbot*, 2004]. The model includes emissions, photochemistry and transport of all major gas phase species (O₃, OH, reactive nitrogen, volatile organics) and gas and aerosol versions of sulfates, nitrates, reactive chlorine and bromine (including aqueous chemistry). The modified version used here retains many of the essential features of CMAQ, including its modular structure,

its representation of atmospheric transport based on results of a mesoscale meteorological model, its link to standard emission inventories and its representation of wet and dry deposition. The major modification involves the numerical solution for aqueous and gas phase chemistry.

[9] The original CMAQ includes separate numerical solutions for changes in concentration fields due to individual atmospheric processes for discrete time intervals, following the standard operator-splitting technique. The combined representation for each 1-h time interval includes calculation of the effects of emissions, horizontal and vertical advection, diffusion, aerosol formation, dry deposition, gas phase and aqueous photochemistry and wet deposition. The solution for gas phase photochemistry uses the standard SMVGEAR solution for an entered list of reactions. The solution for aqueous photochemistry uses methods developed by *Walcek and Taylor* [1986] with a prescribed set of aqueous reactions. Solutions for gas phase and aqueous photochemistry are calculated separately for each 1-h time interval.

[10] The modified version uses an integrated numerical solution for gas phase and aqueous photochemistry [*Sillman*, 1991; *Barth et al.*, 2003] in place of the original gas phase and aqueous solvers. The new procedure solves the implicit (reverse Euler) equations for photochemical production and loss of gas phase and aqueous species using the radical balance method described by *Barth et al.* [2003]. A complete description of the solution procedure is presented here in Appendix A. The procedure has been tested in model intercomparisons for both gas phase and aqueous species [*Olson et al.*, 1997; *Barth et al.*, 2003].

[11] The rate of transfer across the gas-aqueous interface is assumed to be limited by diffusion and is calculated following methods described in *Lelieveld and Crutzen* [1991], assuming a droplet radius of 10 μm and gas diffusivity of 0.1 cm² s⁻¹. Accommodation coefficients are taken from *Lelieveld and Crutzen* [1991] for individual species and assumed to be 0.05 for species (including all mercury species) for which no information is available. The aqueous chemistry calculation includes an adjustment for situations in which the average concentration of an aqueous species is limited by the rate of diffusion within the water droplet, also following methods described by *Lelieveld and Crutzen* [1991].

[12] Aqueous species are not transported independently in the model, and at the end of each time step the aqueous species are converted to the gas phase or aerosol equivalents for transport. In the absence of information about prior aqueous concentrations, we assume that the partitioning between gas and aqueous phase is unchanged during the time step. The aqueous and gas phase concentrations resulting from the combined effect of photochemical production and gas-aqueous exchange is described by the following equation, based on a version from *Lelieveld and Crutzen* [1991]:

$$\frac{dC_g}{dt} = P_g - (L_g + k_t Q)C_g + \frac{k_t}{HRT}C_a \quad (1a)$$

$$\frac{dC_a}{dt} = P_a + k_t Q C_g + \left(L_a + \frac{k_t}{HRT} \right) C_a \quad (1b)$$

where C_a and C_g are aqueous and gas phase concentrations (molecules cm⁻³ air), P_a and P_g are aqueous and gas phase

chemical production rates (molecules cm^{-3} air s^{-1}), L_a and L_g are aqueous and gas phase pseudo-first-order chemical loss rates (s^{-1}), K_H is the Henry's law coefficient (M atm^{-1}), R is the universal gas constant ($\text{L atm mol}^{-1} \text{K}^{-1}$), T (K) is the temperature, Q is the liquid water content ($\text{cm}^3 \text{H}_2\text{O cm}^{-3}$ air), and k_t ($\text{cm}^3 \text{air cm}^{-3} \text{H}_2\text{O s}^{-1}$) is the first-order rate constant that represents diffusion through the gas phase and across the interface of the drop (see *Schwartz* [1986] and *Lelieveld and Crutzen* [1991] for details). In the case of aqueous species linked through fast equilibria (e.g., $\text{HNO}_3(-)\text{H}^+ + \text{NO}_3^-$) C_a , P_a and L_a are replaced by sums for all the linked aqueous species and K_H is replaced by an effective Henry's law coefficient [see, e.g., *Lelieveld and Crutzen*, 1991]. An adjustment is also made to represent situations in which diffusion within the aqueous phase is a limiting factor for aqueous chemistry using methods described by *Lelieveld and Crutzen* [1991].

[13] The above equations yield the following solution for partitioning between the gas and aqueous phase:

$$\frac{C_a}{C_g} = K_H RT Q \frac{P_g + P_a \left(1 + \frac{(L_g + D_g)}{k_t Q} \right)}{P_g + P_a \left(1 + \frac{K_H RT (L_a + D_a)}{k_t} \right)} \quad (2)$$

where D_g and D_a represent $d(\ln C_g)/dt$ and $d(\ln C_a)/dt$ respectively. The assumption that gas-aqueous partitioning does not change during the time step yields the following solution for D_g and D_a :

$$D_g = D_a = \frac{1}{C_g + C_a} \frac{d(C_g + C_a)}{dt} \quad (3)$$

The terms P_g , P_a , L_g , L_a , D_g and D_a are not fully independent of the partition ratio C_a/C_g , but equation (2) can be used as part of an iterative solution for C_a/C_g .

[14] The modified solver is used in place of the original CMAQ solvers for both gas phase and aqueous chemistry. The CMAQ modular structure includes calculation of changes to concentration fields resulting from chemistry production and loss for a given time interval, followed by separate calculation of changes to concentration fields resulting from other physical processes (emissions, advection, deposition, etc.). Alternative solvers for photochemical production and loss can be added with minimal change to the other model components. The calculation of wet deposition was modified to use rainout rates for liquid water derived from the model representation of meteorology along with concentrations of soluble species from the combined gas/aqueous chemistry calculation.

[15] Photolysis rates are derived as a function of altitude, solar zenith angle, albedo, column thickness of ozone, SO_2 and NO_2 , cloud and aerosol optical depths, and time of year. Photolysis rates are calculated off-line using the 8-stream ordinate method from *Madronich and Flocke* [1998]. An interpolation is then used to derive photolysis rates for conditions within the simulation based on the previously tabulated rates, as described by *Feng et al.* [2004]. This calculation is included in the solver for gas/aqueous photochemistry and replaces the original photolysis calculation in CMAQ. In absence of specific information we have used an O_3 optical depth of 340 DU.

[16] The model integration into CMAQ was tested by evaluating changes in concentration fields within the simulation in comparison with directly calculated photochemical production and loss. A direct comparison of CMAQ results for different solvers has not been completed.

[17] The remainder of the model uses standard features of the CMAQ modeling package, including the Fifth Generation Pennsylvania State University/National Center for Atmospheric Research (NCAR) Mesoscale Model (MM5 [*Grell et al.*, 1994]) version 3.6 for meteorology and the Sparse Matrix Operator Kernel Emission (SMOKE) for emissions processing.

[18] MM5 model simulations were initialized using gridded meteorological data fields from the National Centers for Environmental Prediction Final Global Data Assimilation System (FNL), which provides initial conditions to the operational Global Forecast System and Ensemble forecasts. This data set is available at 6-h intervals for 26 vertical levels on a $1^\circ \times 1^\circ$ horizontal resolution. Following the completion of each meteorological simulation, the modeled meteorological fields were compared against the observed data to verify the accuracy of the simulation.

[19] Although CMAQ includes components for modeling aerosol formation, transport and removal, we have not included the formation of particulate mercury in this version. This is a significant omission and may lead to an overestimate of RGM, some of which would otherwise be converted to particulate form. We have also not included natural emission of mercury from soils or the reemission of deposited mercury.

2.2. Photochemical Mechanism

[20] The model chemistry includes gas phase and aqueous reactions for Hg^0 and RGM, derived from *Lin and Pehkonen* [1998a, 1998b, 1999], *Pleijel and Munthe* [1995], *Gardfeldt et al.* [2001], *Sommar et al.* [2001], *Ariya et al.* [2002], *Lindberg et al.* [2002a], *Khalizov et al.* [2003] and *Lin et al.* [2006], including Henry's law and aqueous equilibrium coefficients and interactions between mercury, chlorine, bromine and sulfates. The gas phase reaction of Hg^0 with O_3 is represented with the rate from *Hall* [1995] rather than the faster rate proposed by *Pal and Ariya* [2004]. Aqueous phase reduction of RGM through reaction with HO_2 and O_2^- has been included with rates suggested by *Pehkonen and Lin* [1998]. The viability of the aqueous reduction reactions has been challenged by *Gardfeldt and Jonsson* [2003], and the results include simulations that test the effect of omitting them. Aqueous phase reduction of RGM through the conversion from Hg^{2+} and SO_3^{2-} and reaction to form Hg^0 and SO_2 has been included, as proposed by *van Loon et al.* [2000].

[21] Aqueous reactions for sulfates, nitrates, H_2O_2 , O_3 , OH and related radicals have been taken from *Jacob* [1986], *Pandis and Seinfeld* [1989], *Lelieveld and Crutzen* [1990] and *Liu et al.* [1997]. Reactions of chlorine and bromine are taken from *Sander and Crutzen* [1996] and *Sander et al.* [2003]. Mass accommodation coefficients are based on recommendations from *Lelieveld and Crutzen* [1991]. Auxiliary material¹ contains complete lists of reactions

¹Auxiliary materials are available in the HTML. doi:10.1029/2006JD008227.

Table 1. Model Initial and Boundary Conditions Versus Altitude^a

Species	<500 m	500–4000 m	>4000 m
O ₃	35.	40.	50–70
NO _x	0.03	0.03	0.045–0.015
HNO ₃	0.02	0.1	0.1
PAN	0.12	0.12	0.12
NH ₃	0.1	0.03	0.02
H ₂ O ₂	0.5	1.	0.5
SO ₂	0.2	0.1	0.1–0.01
CO	70.	70.	70.
CH ₄	1400.	1400.	1400.
H ₂	400.	400.	400.
C ₂ H ₆	1.	1.	1.
C ₃ H ₈	1.	1.	1.
NaCl ^b	0.1	0.02	0.01
Cl ₂	0.1	0.05–1e-4	1e-4
Br ₂	1e-5	2e-6	1e-6
HBr	1e-5	2e-6	1e-6
Hg ⁰	2e-4	2e-4	2e-4
RGM	8e-8	8e-8	8e-8

^aUnit is ppb.

^bParticulate NaCl is represented by a gas phase equivalent concentration with high solubility.

and rates for (1) aqueous and halogen photochemistry and (2) mercury photochemistry (also available at <http://www-personal.umich.edu/~sillman/mechanisms2007.htm>).

[22] Gas phase photochemistry includes representation of O₃, reactive nitrogen, CO and a wide range of organics, including organic nitrates and volatile organics from anthropogenic and biogenic sources. The gas phase chemistry is based on the mechanism associated with the GEOS-Chem global model [Evans *et al.*, 2003] with modifications described by Ito *et al.* [2007]. The modifications include the addition of reactions for three representative aromatic species (benzene, toluene and m-xylene) and addition of organic reaction products from the isoprene nitrates.

2.3. Emissions

[23] Anthropogenic emissions for Hg⁰ and RGM were derived from EPA's 1999 version 3 Hazardous Air Pollutants (HAP) [U.S. Environmental Protection Agency (U.S. EPA), 1997a, 2004]. The inventory includes area, point, onroad and nonroad mobile sources. While this inventory has no mercury species for the onroad and nonroad mobile sources, the emissions are all included for other source categories. Speciation into of Hg⁰, RGM, and Hg(p) was done as described by U.S. EPA [1997b]. The same inventory and speciation was used by Bullock and Brehme [2002].

[24] We have not yet included natural emission of mercury from soils or reemission of mercury following deposition. In recent years there has been evidence that soil emission of Hg⁰ in North America contributes significantly to the budget of total gaseous mercury (TGM) and may equal or exceed emissions from anthropogenic sources [Lindberg *et al.*, 2002b; Lin and Tao, 2003; Bash *et al.*, 2004; Lin *et al.*, 2005; Gbor *et al.*, 2006, 2007]. Model results suggest that soil emissions can cause ambient Hg⁰ to increase by 0.2 ng m⁻² [Lin *et al.*, 2005], and inclusion of soil emissions improves agreement with measured TGM [Gbor *et al.*, 2007]. This may represent a significant omission in the current results.

[25] Emissions for other species (NO_x, volatile organics, sulfates) were derived from the 1999 National Emission

Inventory (NEI), version 2 and 3 [U.S. EPA, 2004]. Biogenic emission of volatile organics and NO_x are included.

2.4. Initial and Boundary Conditions

[26] Initial Hg⁰ and Hg⁰ at the model boundary are both set at 1.6 ng m⁻³, which is typical for the background troposphere [Weiss-Penzias *et al.*, 2003; Malcolm *et al.*, 2003]. Initial and boundary RGM are set to a very low value (0.6 pg m⁻³). This insures that RGM in the model is derived almost entirely from model internal emissions and photochemistry rather than from transport from outside the model boundary. We have also omitted temporal and spatial variations in Hg⁰, so that the resulting variation in both Hg⁰ and RGM result from internal model processes. The model does not include episodic transport of elevated Hg⁰ and/or RGM to North America from other continents and omits all other possible sources of variation in Hg⁰ or RGM due to processes external to the model domain.

[27] Other initial and boundary conditions include 40 ppb O₃ (increasing with altitude), based on global average O₃ from Logan [1999]; 0.03 ppb NO_x and 70 ppb CO (see Table 1 for a complete list). Initial and boundary concentrations for halogen in the lower 500 m are set on the basis of estimates for the marine boundary layer from Sander *et al.* [2003]: 0.01 ppb Cl₂ and 0.01 ppt Br₂; and 0.01 ppt HBr. NaCl is represented by assuming an equivalent gas phase concentration of 0.1 ppb. Initial and boundary conditions for these species are decreased by 80% at higher altitudes (see Table 1). Boundary conditions for other species represent typical values for the remote troposphere.

2.5. Model Domain

[28] The model domain (Figure 1) includes the eastern half of the United States and adjacent parts of Canada, most of the Gulf of Mexico, and large parts of the Atlantic Ocean and Caribbean. The domain extends from 15 to 50°N latitude and 55 to 105°W longitude. The domain insures that con-

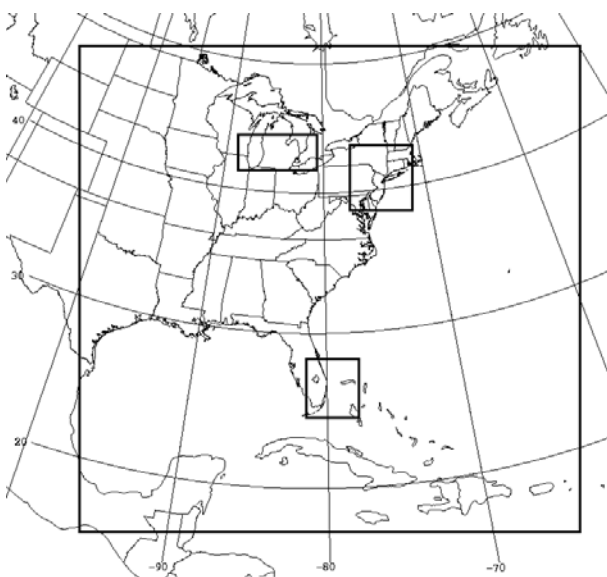


Figure 1. Model horizontal domain. The heavy outlines identify the south Florida, northeast and Great Lakes subregions, which are used for analyzing model output.

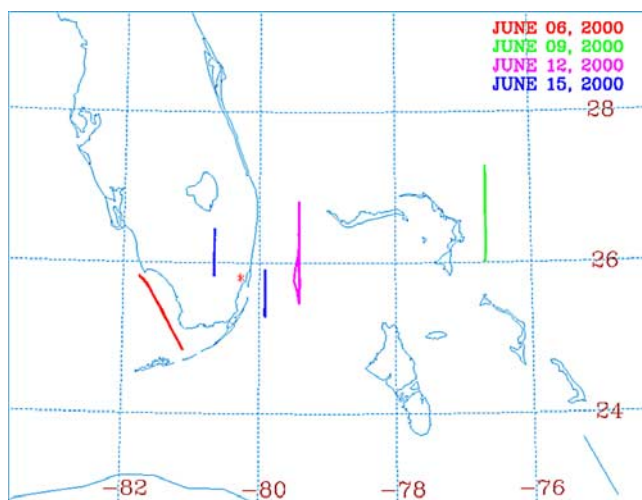


Figure 2. Flight paths for aircraft measurements in Florida on four representative days: 6 June (red line), 9 June (green line), 12 June (pink line), and 15 June (blue line, including two separate paths), all in 2000. The light dotted lines and numbers represent latitudes and longitudes. The asterisk identifies Miami.

ditions in the regions of interest (including Florida and the northeastern United States) reflect calculated photochemistry for several days within the model domain rather than just transport from outside the model boundary. This initial application uses coarse horizontal resolution (36×36 km.) and six vertical layers. The vertical layer boundaries are 0.98, 0.93, 0.84, 0.6 and 0.3 in sigma coordinates (corresponding approximately to 0.1, 0.5, 1.5, 4 and 9 km). The model domain in Figure 1 identifies three subsections (south Florida, the northeast and Great Lakes corridors of the United States) but these are used only for the purposes of displaying model output. The CMAQ structure includes nested grids that allow for more fine resolution in model subsections, but these have not been used here.

[29] Because of the coarse horizontal resolution it is possible that the model underestimates the impact of emissions from local point sources, which are artificially dispersed throughout the 36×36 km grid.

2.6. Measurements

[30] Measurements of Hg^0 and RGM were made from a NOAA Twin Otter aircraft in the vicinity of south Florida during 12 d of flight operations in June 2000, at heights up to 4000 m [Landis *et al.*, 2005]. The aircraft was equipped with a unique shrouded probe inlet and manifold designed specifically for airborne mercury speciation measurements [Irshad *et al.*, 2004]. Five-minute integrated Hg^0 measurements were obtained using collocated Tekran Instruments Corporation (Knoxville, Tennessee) Model 2537A mercury vapor analyzers with KCl-coated multichannel annular denuders incorporated into the inlet system to prevent collection of RGM. RGM was collected using collocated manual KCl-coated annular denuders that were subsequently analyzed in a mobile laboratory at the airport immediately following aircraft operations using a method described by Landis *et al.* [2002]. RGM measurements were integrated along each flight trajectory. All mercury results have been

corrected to standard temperature and pressure and are reported as units per standard cubic meter. Measured O_3 , CO, NO and NO_2 were also available at 5-min intervals along the flight paths.

[31] The majority of the flight paths (for 3, 12, 14, 18, 25 and 26 June) were over the Atlantic Ocean along the Florida coast, 50 km east of the Miami metropolitan area. Two days (15 and 21 June) also included a flight path over the Everglades. Two days (4 and 6 June) had measurements over the Gulf of Mexico 50 km west of the Everglades, and 2 d (9 and 22 June) had measurements over the Atlantic Ocean in the vicinity of the Bahamas, 250 km east of Miami. Figure 2 shows the flight path for 4 d (6, 9, 12 and 15 June). Flight paths on the other days were all similar to the paths on one of the days appearing in Figure 2. All measurements were during the afternoon hours, and most were for the hours 1600 to 1800 local time (LT).

2.7. Simulated Events and Meteorology

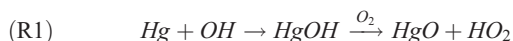
[32] The model has been used to simulate events for 8–14 June and 23–26 June 2000, with a spin-up period of 2 d before the start of each event. These time periods include 5 d that coincide with aircraft-based measurements in south Florida (9, 12, 14, 25 and 26 June), including the days with the highest measured ambient RGM (12 and 14 June). Because of the short spin-up time it is possible that the model will underestimate the amount of RGM resulting from conversion from Hg^0 .

[33] The model time period also includes a variety of meteorological conditions that might affect conditions in Florida. These include (1) several days with extensive transport from the east (representing the prevailing circulation pattern) and photochemical processing for several days over the Atlantic Ocean prior to arrival in Florida; (2) an event with characteristic Bermuda High circulation over the Atlantic Ocean (12 June) that might result in transport from the northeastern United States to Florida; and (3) an event (9 June) with direct transport into Florida from the north, which might lead to transport of pollutants to Florida from the midwestern United States. The simulated events also coincide with a variety of conditions in the northeast and midwestern United States, including periods with extensive rain (12 and 14 June) and periods with stagnant circulation and elevated O_3 (25 and 26 June).

3. Chemistry of Atmospheric Mercury

[34] The proposed reactions of mercury (see references in section 2.2) suggest the following cycle of mercury in the atmosphere.

[35] Hg^0 is converted into RGM primarily by gas phase reactions with OH and O_3 .



[36] On the basis of global average concentrations of OH (1.16×10^{-6} mol cm^{-3} , from Spivakovsky *et al.* [2000]) and O_3 (40 ppb [Logan, 1999]), the chemical lifetimes of Hg with

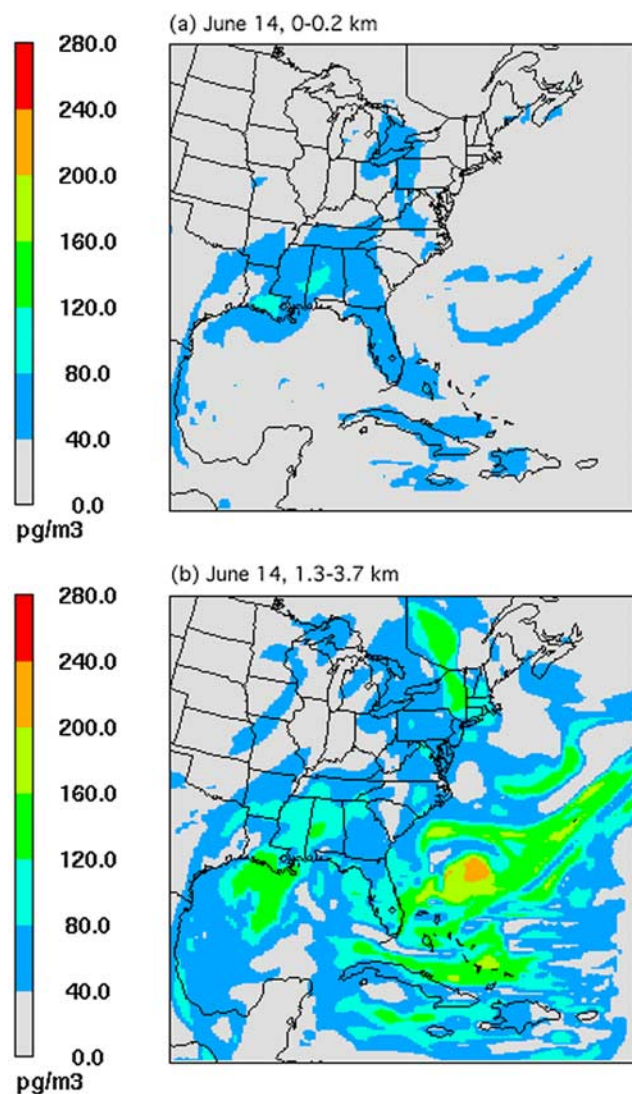


Figure 3. Model ambient concentrations of reactive mercury (RGM) in pg m^{-3} on 14 June 2000 at 1700 LT for (a) the model surface layer (0–200 m) and (b) an aloft layer (1.3–3.7 km). Shadings represent intervals of 40 pg m^{-3} extending from 0 to 280 pg m^{-3} .

respect to these reactions are 115 d for $\text{Hg} + \text{OH}$ and 390 d for $\text{Hg} + \text{O}_3$. The $\text{Hg} + \text{OH}$ reaction, proposed by Sommar *et al.* [2001], appears to be the dominant gas phase reaction. The chemical lifetime of Hg may be considerably faster than 115 d in the lower troposphere in tropical regions and in the midlatitude summer, where average OH are 2–3 times higher than the global average [Spivakovsky *et al.*, 2000].

[37] Ariya *et al.* [2002], Khalizov *et al.* [2003], Calvert and Lindberg [2003, 2004], Sumner *et al.* [2005], and Lin and Pehkonen [1998b] have also suggested that gas phase reactions with halogens (Cl_2 , Cl, Br, I and HOCl) may convert significant amounts of Hg^0 to reactive forms (HgCl_2 , HgCl , HgBr and HgI respectively). Ariya *et al.* found that the reaction with Br can convert Hg^0 to reactive forms on timescales as fast as 2 d in the Arctic marine boundary layer. Outside the Arctic the chemical lifetime of Hg^0 with respect to the reaction with Br is 15 d in the marine

boundary layer, based on estimated Br (10^{-5} ppb) from Sander and Crutzen [1996]. The lifetime of Hg^0 with respect to the other chlorine and bromine reactions is 500 d or longer, also based on marine concentrations from Sander and Crutzen [1996] (10^{-2} ppb Cl_2 , 10^{-7} ppb Cl and 10^{-2} ppb Br_2).

[38] Conversion of Hg^0 to RGM also occurs through the aqueous phase reaction of Hg^0 with O_3 , equivalent to R1 above. Hg^0 and O_3 are both slightly soluble in water with typical concentrations of $2\text{e-}14 \text{ M Hg}^0$ (corresponding to 1.5 ng m^{-3} or 0.2 ppt in the gas phase) and $4.3\text{e-}10 \text{ M O}_3$ (corresponding to 40 ppb). This results in a chemical lifetime of 50 s for Hg^0 within cloud droplets, but the significance of the removal process is limited by the fraction of total $\text{Hg}(0)$ in the aqueous phase. For a typical cloud liquid water content (LWC) of $0.3 \times 10^{-6} \text{ g cm}^{-3}$ within clouds [e.g., Pruppacher and Klett, 1997] the chemical lifetime of Hg^0 (including both gas phase and aqueous) with respect to the aqueous $\text{Hg}^0 + \text{O}_3$ reaction is 700 d. Cloud water content in large thunderstorms can reach $1 \times 10^{-5} \text{ gm cm}^{-3}$, corresponding to a chemical lifetime of 20 d with respect to the aqueous $\text{Hg}^0 + \text{O}_3$ reaction. Therefore this reaction is unlikely to be significant.

[39] The most important aqueous reactions are the reduction of RGM through reaction with HO_2 or O_2^- . These reactions, identified by Pehkonen and Lin [1998], have the potential to convert RGM to Hg^0 rapidly. Assuming a typical concentration of $\text{HO}_2 + \text{O}_2^-$ of $1\text{e-}8 \text{ M}$ [DeGuillaume *et al.*, 2003; Monod and Carlier, 1999] along with reaction rates identified by Pehkonen and Lin [1998] the lifetime of RGM would be less than 2 h. As will be described below, these reactions have a large impact on model calculations. However, Gardfeldt and Jonsson [2003] challenged the viability of this reaction, suggesting instead that reduction of RGM is accomplished through photolysis of organic ligands that form from RGM and oxalic acid. van Loon *et al.* [2000] also proposed that the aqueous compounds HgSO_3 might dissociate to form Hg^0 . This study has included the reduction of RGM through reaction with HO_2 and O_2^- but not the dissociation of HgSO_3 .

4. Results

4.1. Model Results

[40] Figure 3 shows simulated RGM at two altitude layers (0–0.2 km and 1.3–3.7 km) over the full model horizontal domain. The most striking feature of Figure 3 is the elevated RGM at 1.3–3.7 km, especially over the Atlantic Ocean on 14 June. The highest RGM (230 pg m^{-3}) appears over the Atlantic Ocean east of Florida. Similar elevated RGM appears on all model days, and the maxima usually are found over the Atlantic Ocean. RGM shows a spatially heterogeneous pattern with elevated values ($>120 \text{ pg m}^{-3}$) and low values ($<40 \text{ pg m}^{-3}$) occurring simultaneously over horizontal distances of 100 km or less. Although high RGM also appears over the midwestern United States on one day (9 June), RGM is more often high over the Atlantic Ocean.

[41] The geographical pattern of RGM is very different near the surface. Ambient RGM is much lower in the 0–0.2 km model layer compared to the 1.3–3.7 km layer. The highest RGM at 0–0.2 km occurs over the continental United States, possibly reflecting greater vertical mixing over the continent.

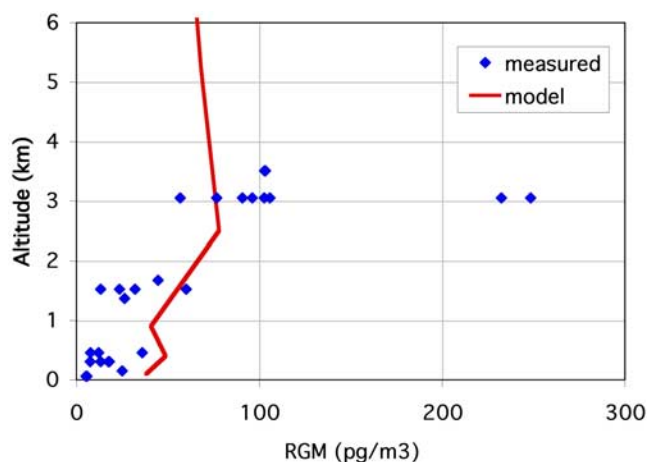


Figure 4. Measured RGM (pg m^{-3}) versus altitude (km) from aircraft measurements over the Atlantic Ocean off the coast of south Florida during June 2000 (points). The line represents model RGM versus altitude, based on an average of model results during the afternoon on the 5 d (9, 12, 14, 25 and 26 June) that coincide with measurements.

[42] The geographical variation of ambient RGM in the model is due primarily to the spatial pattern of clouds and the influence of aqueous removal of RGM. Regions with low RGM coincide with clouds, and the highest RGM occurs in air masses with a long cloud-free history. We have tested this by adding a model tracer that is accumulated at a rate proportional to the model OH concentration and is removed instantaneously by contact with cloud droplets. This model tracer shows the same geographical variation as RGM (see section 5).

[43] The geographical pattern for RGM shows little relation to the location of emission sources, in contrast to other anthropogenic species (NO_x , sulfates, O_3) that typically have highest values near or downwind from emission sources.

4.2. Comparisons With Measurements

[44] Figures 4 and 5 show comparison between model ambient RGM and measured values from the aircraft flights described in section 2.6. Figure 4 shows the variation of RGM with altitude in the model for the 5 d that correspond with measurements (9, 12, 14, 25 and 26 June, always at 1700 LT). Figure 4 also shows measured RGM versus altitude for the full ensemble of measurements during June 2000, including days not represented by the model. The full set of measurements is included here in order to show a complete picture of the observed variation with height.

[45] Results show that the model is consistent with measurements in many aspects, although there are also significant discrepancies. RGM increases with altitude from 0 to 3 km in both the model and in the measured ensemble. The rate of increase versus altitude is steeper for the ensemble of measurements than for the model, but the comparison is not extensive enough to show whether this is a consistent trend. Individual vertical profiles of RGM in the model sometimes show a complex layered pattern, reflecting cloud layers at various elevations, but the measurements represent flight path averages and cannot show this type of detail.

[46] A direct comparison between model and measured values (paired in time and space) is possible for a subset consisting of nine measurements over 5 d (see Figure 5). For this subset the range of model and measured values are similar ($15\text{--}126 \text{ pg m}^{-3}$ modeled, $8\text{--}248 \text{ pg m}^{-3}$ measured).

[47] The model shows a large underestimate in comparison with the highest measured RGM (232 and 248 pg m^{-3} measured on 12 and 14 June, compared to 87 and 126 pg m^{-3} modeled), and at high altitudes in general. However, the model prediction includes RGM up to 233 pg m^{-3} on these days at other locations over the Atlantic Ocean near Florida (see Figure 3). Although not tested directly, the day-to-day variation in measured RGM near Florida (from 60 to 248 pg m^{-3} at 3 km) is qualitatively similar to the spatially intermittent pattern of high and low RGM over the Atlantic Ocean found in the model.

[48] In terms of EPA performance statistics for the subset of nine measurements, the model shows a normalized bias of -0.08 and a normalized gross error of 0.56 . This is somewhat misleading because the normalized discrepancy is dominated by a single measurement with very low RGM

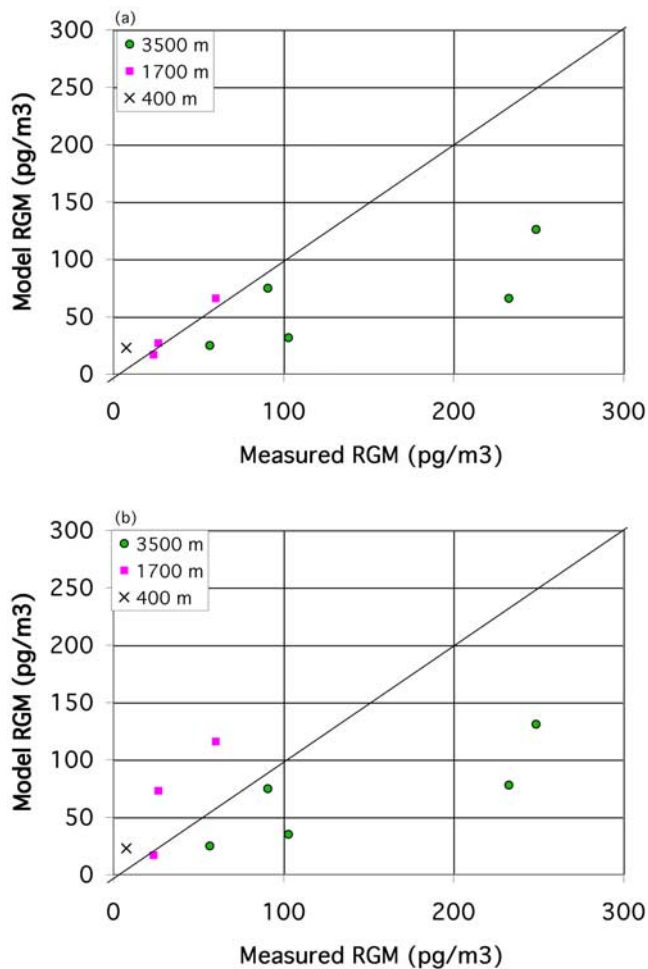


Figure 5. Model versus measured RGM (pg m^{-3}) paired in time and space for 9, 12, 14, 25 and 26 June, shown for (a) the model base case and (b) the model scenario with the aqueous reactions of RGM with HO_2 and O_2^- omitted. Results are sorted by altitude: 3000–3500 m (circles), 1400–1700 m (squares) and 0–400 m (crosses).

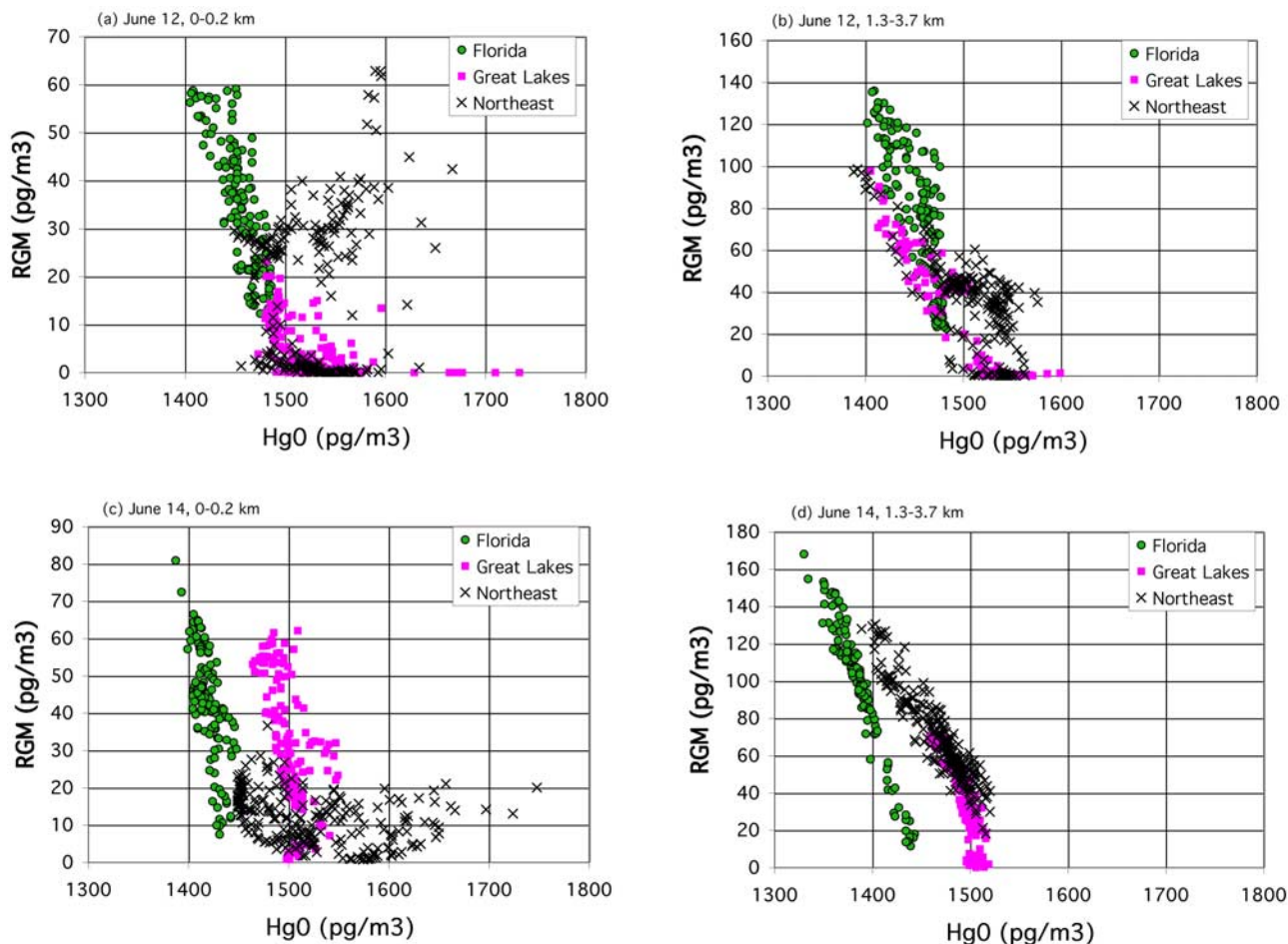


Figure 6. Model correlation between Hg^0 and RGM in pg m^{-3} for the south Florida (green circles), northeast (crosses) and Great Lakes (pink squares) subregions identified in Figure 1. Correlations are for (a) 12 June, 0–0.2 km altitude; (b) 12 June, 1.3–3.7 km; (c) 14 June, 0–0.2 km; and (d) 14 June, 1.3–3.7 km, all at 1700 LT.

(7 pg m^{-3} measured, 23 pg m^{-3} modeled). If this measurement is omitted the resulting normalized bias is -0.35 and the normalized gross error is 0.38 .

4.3. Processes, Sensitivities, and Species Correlations

[49] Formation of RGM results from two contrasting processes: direct emission of RGM, usually from relatively local anthropogenic sources; and photochemical conversion from Hg^0 through either gas phase or aqueous photochemistry. The impact of these processes can be identified in model simulations through sensitivity tests with one process reduced or removed. Results of sensitivity tests will be shown here. Along with the sensitivity tests, we will also show model results for correlations between ambient species. As will be shown here, the predicted species correlations are often closely related to model processes and sensitivity predictions. Results will be presented for three model subregions: southern Florida and the nearby ocean; the northeast corridor including Washington D.C., New York and Boston (also including the nearby ocean); and the Great Lakes corridor including Chicago, Detroit, Cleveland, Toronto and adjacent rural areas (see Figure 1).

[50] Figure 6 shows the model correlation between Hg^0 and RGM in the three selected regions. On 12 June at 0–

0.2 km Hg^0 and RGM in south Florida are anticorrelated ($r^2 = 0.67$). The total gaseous mercury ($\text{TGM} = \text{Hg}^0 + \text{RGM}$, not shown directly in Figure 6) remains nearly constant. By contrast, Hg^0 and RGM are positively correlated over parts of the northeast. The correlation coefficient is low ($r^2 = 0.04$) because of the large number of model locations with near-zero RGM. If results are limited to the subset of model locations in the northeast with RGM above 10 pg m^{-3} the statistical correlation is stronger ($r^2 = 0.27$).

[51] Model results show that the contrasting correlation patterns for Hg^0 versus RGM are linked to the model predictions for the source of RGM. When the model predicts that RGM is produced primarily through photochemical conversion from Hg^0 , it also predicts a negative correlation between ambient RGM and Hg^0 . When the model predicts that RGM is due primarily to direct emissions, it also predicts a positive correlation between ambient RGM and Hg^0 . The linkage between correlation patterns and predicted model sensitivity is shown in Figure 7. When the model is exercised with zero emission of RGM and Hg^0 within the model domain (so that RGM is produced solely from photochemical conversion from background Hg^0) the elevated RGM in the northeast is greatly reduced, and the

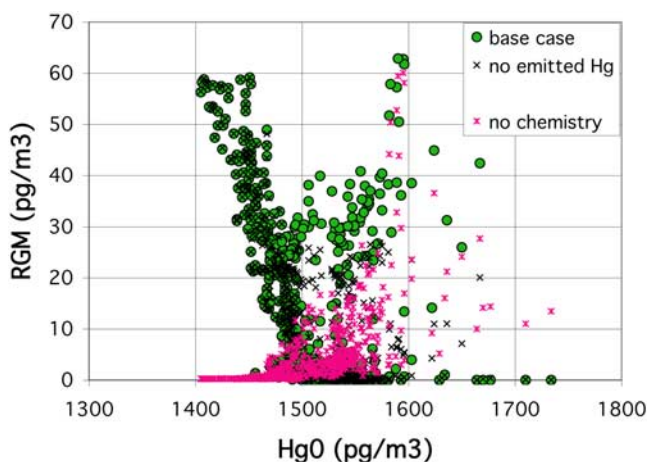


Figure 7. Sensitivity of RGM to model processes. The green circles show the model correlation between Hg^0 and RGM in pg m^{-3} for the south Florida, northeast and Great Lakes subregions on 12 June, 1700 LT, 0–0.2 km altitude (equivalent to Figure 6a). The crosses show Hg^0 versus RGM in a model with a no direct emission of Hg^0 or RGM. The pink asterisks show Hg^0 versus RGM in a model with no photochemical production or loss of Hg^0 or RGM.

remaining RGM is not positively correlated with Hg^0 . When the model is exercised without photochemical conversion between RGM and Hg^0 (so that RGM is derived from either direct emissions or from the near-zero initial and boundary RGM) the model ambient RGM in Florida is reduced to near zero, and the negative correlation between ambient RGM and Hg^0 no longer appears. When the model is exercised with zero initial and background Hg^0 and RGM (not shown) results are similar to the case with photochemistry omitted. In this scenario the model Hg^0 and RGM are both derived entirely from emissions within the model domain. The elevated RGM in Florida is again reduced to near zero and the negative correlation between RGM and Hg^0 disappears.

[52] The pattern of positive and negative correlation between Hg^0 and RGM, described above for 12 June, shows significant day-to-day variation. On 14 June the predicted near-surface RGM in the northeast remains low ($<20 \text{ pg m}^{-3}$) and does not show a positive correlation with Hg^0 , possibly because the directly emitted RGM is largely removed by aqueous reduction of RGM in clouds. The Great Lakes region has higher RGM (up to 60 pg m^{-3} , comparable to the northeast on 12 June) but with a slight anticorrelation between Hg^0 and RGM ($r^2 = 0.33$). Similar variations in the predicted surface correlation patterns in the northeast and midwest occur on other days. By contrast, Hg^0 and RGM at 1.3–3.7 km are predicted to anticorrelate in all three regions and on all model days. There is little impact of direct emissions at this altitude, which is above the daytime mixed layer in the model. Hg^0 and RGM also are predicted to anticorrelate on all days in Florida, even at the surface.

[53] The above results suggest that a comparison with the measured correlation for Hg^0 versus RGM is a useful way to evaluate whether models are correctly representing the source of RGM. Figure 8 shows the measured correlation between Hg^0 and RGM and between total gaseous mercury (TGM) and RGM based on the ensemble of aircraft mea-

surements in south Florida during June 2000. Hg^0 and RGM anticorrelate throughout both these sets of measurements, but there are important differences between the measured correlation and model predictions shown in Figure 6. The measurements showed a significant anticorrelation between RGM and TGM as well as between RGM and Hg^0 . By contrast, the model predicted an anticorrelation between RGM and Hg^0 but not between RGM and TGM. The measured pattern cannot be clearly attributed to conversion from Hg^0 to RGM because this process does not explain the anticorrelation between RGM and TGM. Model values corresponding to the June measurements on days included in the model are also shown in Figure 8 and illustrate the difference between the measured and model correlation. The measured anticorrelations might be explained by a process of conversion from Hg^0 to both RGM and $\text{Hg}(\text{p[O]})$, but only if $\text{Hg}(\text{p})$ greatly exceeded RGM. Measurements also show

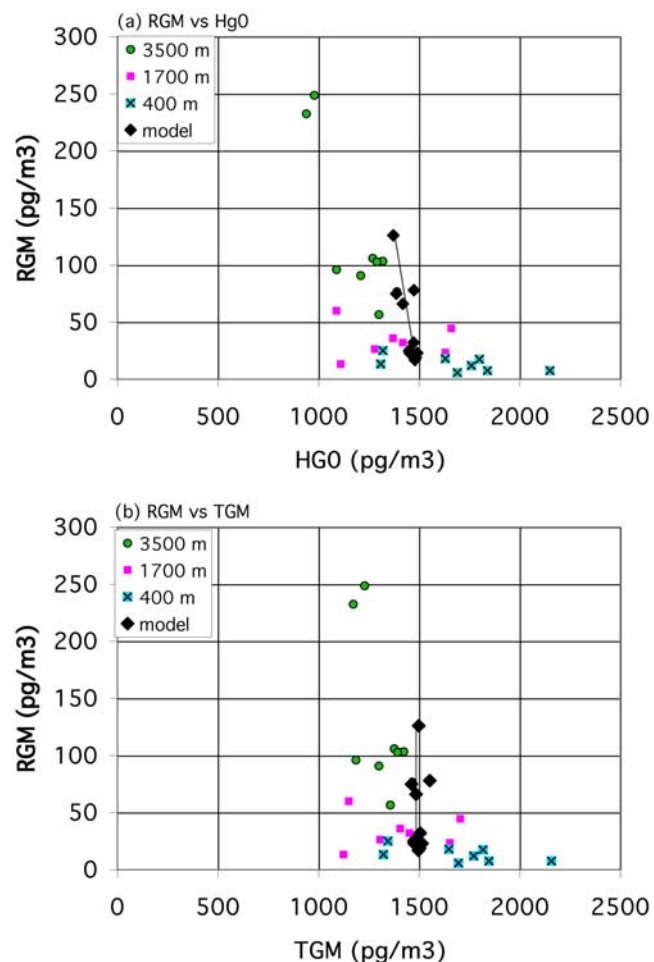


Figure 8. Measured correlation between RGM and (a) Hg^0 and (b) TGM, both in pg m^{-3} , from the full ensemble of flight measurements during June 2000. Results are sorted by altitude: 3000–3500 m (circles), 1400–1700 m (pink squares) and 0–400 m (blue crosses). The black diamonds and connecting line represent model values corresponding to the subset of measurements included in the model time period.

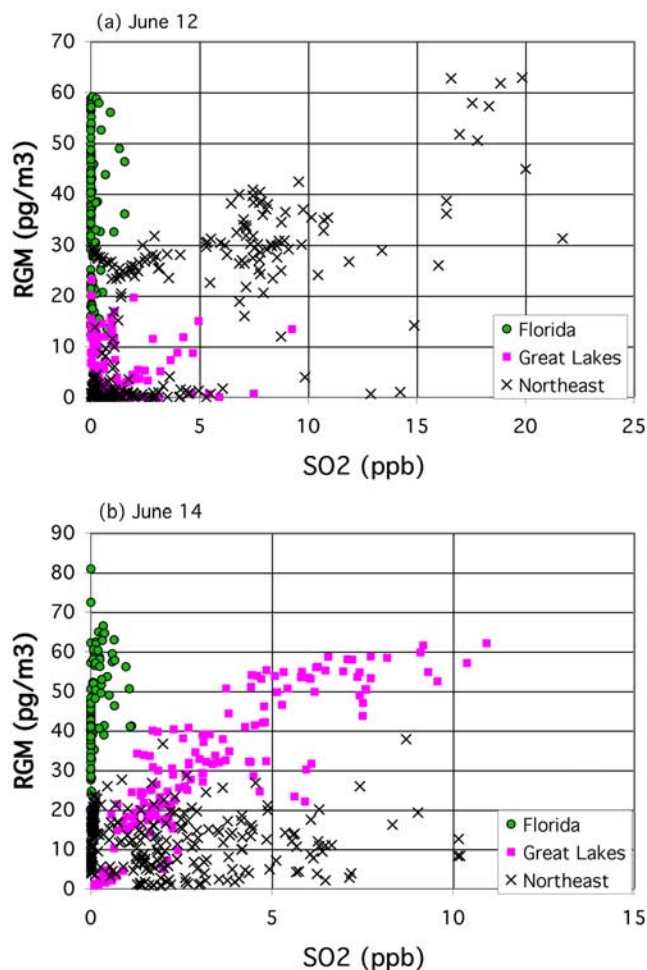


Figure 9. Model correlation between RGM (pg m^{-3}) and SO_2 (ppb) for the south Florida (green circles), northeast (crosses) and Great Lakes (pink squares) subregions identified in Figure 1. Correlations are for (a) 12 June and (b) 14 June, both at 0–0.2 km altitude and 1700 LT.

significantly higher Hg^0 during January (2.2 ng m^{-3}) than in June (1.4 ng m^{-3}), although RGM was higher in June.

[54] The slope for RGM as a function of Hg^0 , calculated on the basis of least squares fits, varies from -0.5 to -0.9 on individual days in Florida in the model at 0–0.2 km and between -0.9 and 1.5 at 1.3–3.7 km. The slope for the measured RGM versus Hg^0 in Florida is much lower (-0.15). Perhaps coincidentally, Swartzendruber *et al.* [2006] reported a slope of 0.87 for RGM versus Hg^0 at the Mount Bachelor site in Oregon, a value comparable to the model results for Florida.

[55] The influence of direct emissions on ambient RGM concentrations can sometimes be identified through correlations between RGM and either sulfur dioxide (SO_2) (Figure 9) or total reactive nitrogen (NO_y), although both species are imperfect tracers for anthropogenic influence. SO_2 has been widely used as a tracer for emissions from large coal-fired sources [e.g., Ryerson *et al.*, 1998], but recent efforts at pollution control in the United States have sharply reduced SO_2 emissions from some sources. Additionally, correlations between RGM and both SO_2 and NO_y are imperfect because emission sources of the three species

do not necessarily coincide. As described in section 4.4, positive correlations between RGM and either SO_2 or NO_y also can occur when RGM is linked to chemistry associated with elevated O_3 rather than to direct emissions. As shown in Figure 9 a positive correlation between RGM and SO_2 is predicted in the northeast on 12 June (apparently linked with direct emissions of RGM) and in the Great Lakes region on 14 June (apparently linked to the influence of elevated O_3 as described in section 4.4).

[56] Photochemically produced RGM can sometimes be identified through correlations between RGM and hydrogen peroxide (Figure 10), but this correlation is also imperfect. Ambient H_2O_2 shares some important features with photochemically produced RGM. RGM and H_2O_2 have similar lifetimes in the troposphere (3–5 d), are both produced from reactions involving odd hydrogen radicals and are both removed by wet deposition and through aqueous photochemistry. However, the formation of H_2O_2 increases quadratically with HO_2 , whereas photochemical formation of RGM increases linearly with OH . A correlation between RGM and H_2O_2 is predicted for south Florida on all days at

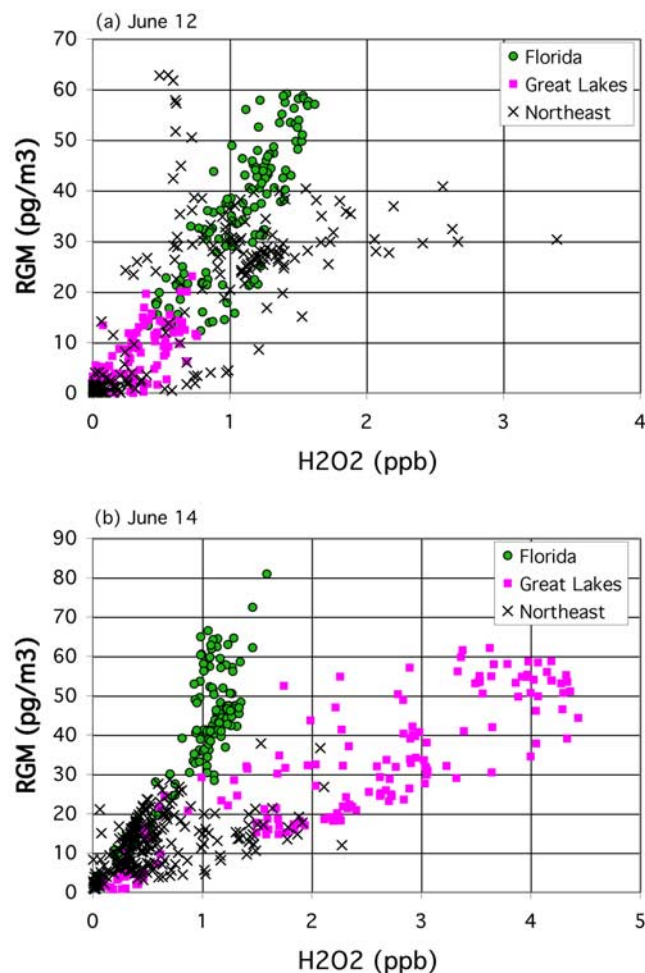


Figure 10. Model correlation between RGM (pg m^{-3}) and H_2O_2 (ppb) for the south Florida (green circles), northeast (crosses) and Great Lakes (pink squares) subregions identified in Figure 1. Correlations are for (a) 12 June and (b) 14 June, both at 0–0.2 km altitude and 1700 LT.

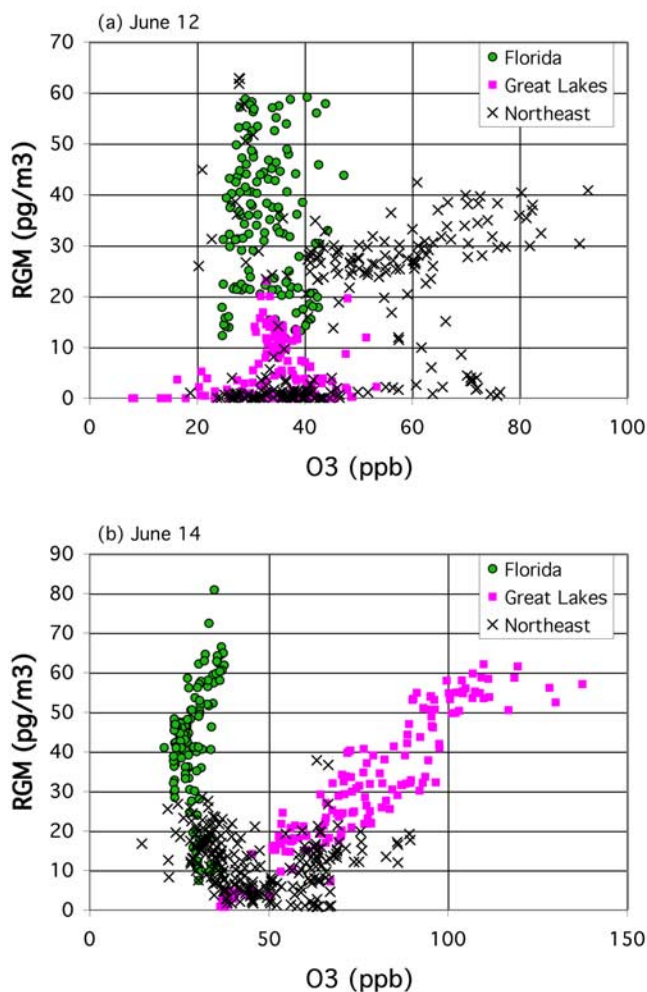


Figure 11. Model correlation between RGM (pg m^{-3}) and O_3 (ppb) for the south Florida (green circles), northeast (crosses) and Great Lakes (pink squares) subregions identified in Figure 1. Correlations are for (a) 12 June and (b) 14 June, both at 0–0.2 km altitude and 1700 LT.

0–0.2 km (with slope 35–45 $\text{pg m}^{-2} \text{ppb}^{-1}$), and a similar correlation with a steeper slope (80–100 $\text{pg m}^{-2} \text{ppb}^{-1}$) is predicted at 1.3–3.7 km. By contrast, the predicted correlation in the northeast is weak or nonexistent. A correlation between H_2O_2 and RGM is also predicted for the Great Lakes region, but with a lower slope on 14 June (12 $\text{pg m}^{-2} \text{ppb}^{-1}$). The lower slope in the Great Lakes region on 14 June reflects conditions in a source region with elevated O_3 and high photochemical activity, and may occur because high biogenic emissions and high rates of the $\text{O}^1\text{D} + \text{H}_2\text{O}$ reaction lead to very high HO_2 and H_2O_2 [e.g., *Weinstein-Lloyd et al.*, 1998]. These variations are related primarily to the complex photochemistry of H_2O_2 rather than to RGM.

[57] It is worth noting that the ambient RGM is also critically sensitive to the initial and boundary condition for total gaseous mercury (here, almost entirely Hg^0). The lifetime of Hg^0 is too long for representation in a regional-scale model, and the magnitude of Hg^0 is determined mainly by the initial and boundary conditions. When RGM is formed through photochemical conversion from Hg^0 its magnitude is also affected by the initial and boundary Hg^0 .

We have found that a 50% increase in initial and boundary Hg^0 results in a 50% increase in ambient RGM in most of the model domain. RGM is unaffected by boundary conditions only in locations where ambient RGM is derived from local emissions. There is no qualitative change in the model correlations between RGM and other species, but the correlation slopes change consistently with the above description.

4.4. Ozone and Reactive Mercury in Polluted Regions

[58] Model results suggest that enhanced O_3 during pollution events can also cause increases in concentrations of ambient RGM.

[59] Figure 11 shows the predicted surface correlation between O_3 and RGM for Florida, the northeast and Great Lakes corridors. The simulation included region-wide pollution events with elevated O_3 in both the northeast and Great Lakes. During these events RGM was often strongly correlated with ambient O_3 during the afternoon. The correlation is seen most strongly in the Great Lakes region on 14 June (see Figure 11). Similar strong correlations were predicted for both the northeast and Great Lakes regions on other days. Results from 12 June show a different pattern with no correlation between RGM and O_3 , despite the presence of elevated O_3 in the northeast. No correlation between O_3 and RGM was ever found in Florida, where O_3 remains at near-background levels (40 ppb) throughout the simulation. The positive correlation between RGM and O_3 on 14 June in the Great Lakes region also coincided with positive correlations between RGM and ambient markers for anthropogenic influence (SO_x , NO_y) and between RGM and H_2O_2 .

[60] The strong correlation between O_3 and RGM suggests that the photochemistry associated with enhanced O_3 may also lead to increased conversion from Hg^0 to RGM. Alternately, the correlation between O_3 and RGM may be coincidental, because of the collocation of emission sources of RGM and ozone precursors and the higher concentrations of emitted pollutants during stagnation events. We have tested these possibilities by repeating the simulation with a 99% reduction in emissions of both NO_x and anthropogenic VOC. This has the effect of reducing O_3 to near-background levels throughout the model domain.

[61] Results (Figure 12) suggest that RGM is affected by anthropogenic NO_x and VOC in the Great Lakes region during pollution events, but not in Florida. Ambient RGM is reduced by up to a factor of two in the Great Lakes region when anthropogenic NO_x and VOC are removed. A similar reduction in RGM was predicted in the northeast on a different day (9 June) that coincided with elevated O_3 in that region. Ambient RGM does not appear to be affected by anthropogenic NO_x or VOC in Florida, where O_3 remained low throughout the simulation.

[62] Model results also suggest that the correlation between RGM and O_3 during pollution events is driven largely by the effect of elevated O_3 and its precursors on photochemical production of RGM. The alternative case in Figure 12 represents the RGM that would result if there were no enhancement of photochemical production of RGM due to anthropogenic NO_x , VOC or O_3 . The resulting ambient RGM still shows a significant correlation with O_3 in the Great Lakes subregion ($R^2 = 0.74$), suggesting that some of the predicted correlation is due to meteorological factors that favor simultaneous production of both species.

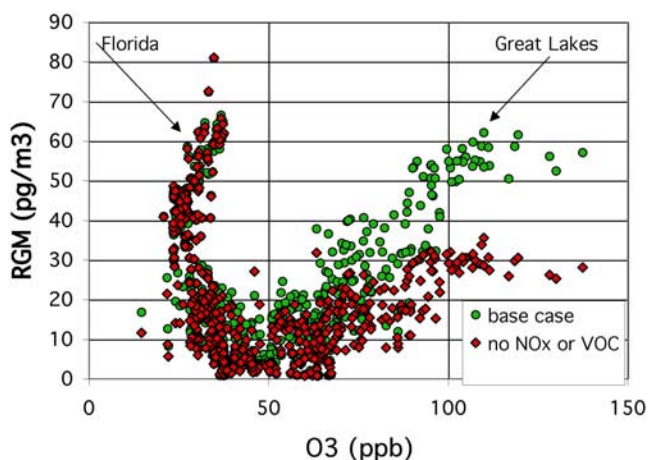


Figure 12. Relation between model RGM and O_3 . The green circles show the model correlation between RGM (pg m^{-3}) and O_3 (ppb) for the south Florida, northeast and Great Lakes subregions at 1700 LT, 14 June, 0–0.2 km altitude (equivalent to Figure 11b). The red diamonds show RGM in a model with a 99% reductions in anthropogenic VOC and NO_x (resulting in O_3 close to background values throughout the simulation), plotted against O_3 in the model base case.

However, the correlation between RGM and O_3 is stronger in the original scenario ($R^2 = 0.86$) and the predicted slope between RGM and O_3 is twice as high ($0.71 \text{ pg m}^{-2} \text{ ppb}^{-1}$ versus $0.33 \text{ pg m}^{-2} \text{ ppb}^{-1}$). Thus a correlation between RGM and O_3 would still be present even if there were no causal relationship between them, but the predicted correlation is much stronger in models that include a causal relationship.

[63] It is useful to contrast the correlations for RGM, Hg^0 and O_3 in the Great Lakes region on 14 June with the different correlation patterns in the northeast on 12 June (see Figures 6 and 11). Model results for the northeast on 12 June show a positive correlation between RGM and Hg^0 but no correlation between RGM and O_3 , despite the presence of elevated O_3 (up to 80 ppb) in the region. Model sensitivity tests predicted that ambient RGM during this event was affected by direct emissions of RGM, but that emission of ozone precursors (NO_x and VOC) had relatively little impact. By contrast, results for 14 June in the Great Lakes showed a strong correlation between RGM and O_3 and a slight negative correlation between RGM and Hg^0 . Model sensitivity tests suggested that ambient RGM was influenced by emissions of ozone precursors, but that direct emission of RGM had a minor impact on RGM. These contrasting patterns may provide a basis for evaluating the accuracy of model predictions concerning the impact of precursor emissions on RGM.

5. Discussion and Interpretation

[64] The spatially complex model results for RGM, illustrated in Figure 3, result from the major photochemical processes that affect RGM in the model. Hg^0 is slowly converted to RGM through gas phase reactions, primarily with OH. RGM is removed rapidly when clouds form,

either through rainout or through aqueous reactions that reduce RGM to Hg^0 . Elevated RGM occurs in air masses with an extensive cloud-free history along its transport path. Although elevated RGM occurs sometimes in cloud-free stagnation episodes with elevated O_3 (for example, on 9 June in the midwestern United States in Figure 3), the high RGM over the Atlantic Ocean in the model occurs as part of general atmospheric circulation with intermittent clouds.

[65] In order to clarify the process further we have added a tracer that represents cloud-free exposure to OH. The OH tracer in the model is produced at a rate proportional to the model gas phase OH concentration and is removed rapidly by exposure to liquid water in clouds. The tracer is treated as a photochemically active species with very high solubility in water and rapid removal through aqueous pseudo-reactions. Effectively it represents the accumulated exposure to OH of a given air mass (in ppb-hours or equivalent units) since its last exposure to a cloud.

[66] Figure 13 shows the spatial variation in the OH tracer on 14 June at the same time as the RGM shown in Figure 3. A comparison between Figures 14 and 3 shows that the OH tracer captures most of the spatial variation in RGM. The maximum RGM in the model over the Atlantic Ocean and secondary maxima over the Gulf of Mexico and north of New York all correspond to maxima in the OH tracer. The regions with low RGM, including the midwestern United States, the North Atlantic off Maine and Nova Scotia, and the Yucatan in Mexico, all correspond to low values for the OH tracer. The model RGM is strongly correlated with the OH tracer except in locations in which RGM was affected by local emissions or by dry deposition, both of which were not included in the tracer simulation.

[67] It is useful to compare these results with the global analysis from Selin *et al.* [2007]. Selin *et al.* found that the highest model RGM is associated with subsidence events and that a pool of elevated RGM ($>200 \text{ pg m}^{-3}$) forms in the upper troposphere above 10 km and in the stratosphere.

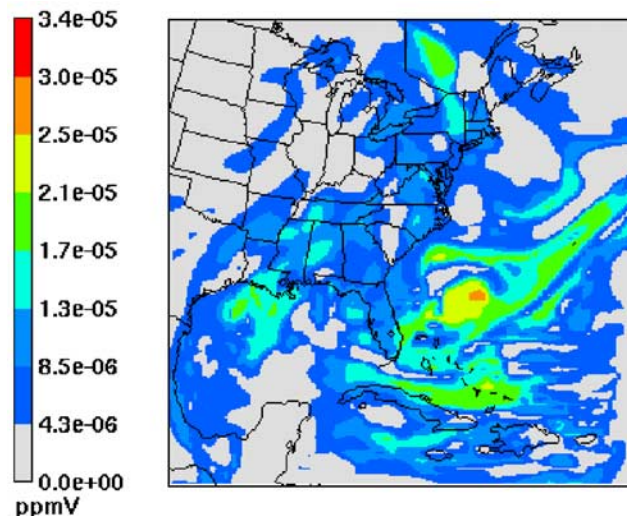


Figure 13. Model ambient concentrations of the OH tracer (in ppm h) on 14 June 2000 at 1700 LT for a model aloft layer (1.3–3.7 km). Shadings represent intervals of 40 pg m^{-3} extending from 0 to $3.4 \times 10^{-5} \text{ ppm h}$.

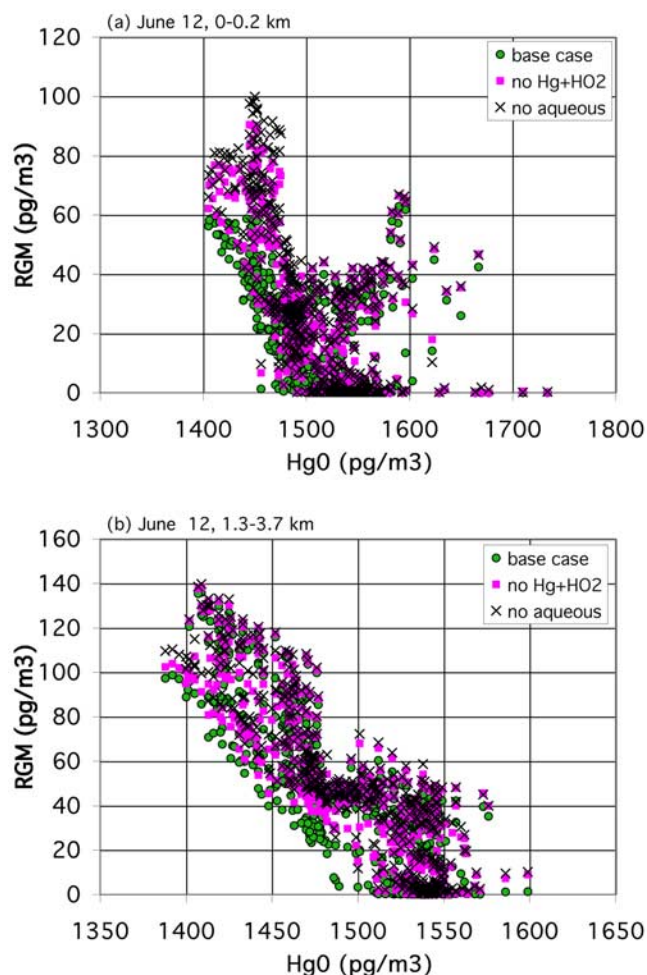


Figure 14. Sensitivity to model chemistry. The green circles show the model correlation between Hg^0 and RGM in pg m^{-3} for the south Florida, northeast and Great Lakes subregions on 12 June, 1700 LT, (a) 0–0.2 km altitude and (b) 1.3–3.7 km (equivalent to Figures 6a and 6b). The pink squares show results from a simulation with the aqueous reaction of RGM with HO_2 and O_2^- removed. The crosses show results from a simulation with all aqueous reactions removed.

Because subsidence events are associated with extended cloud-free periods in the lower troposphere the highest RGM may be due to a combination of transport from the upper troposphere and continuing photochemical production in the lower troposphere. Here, we have modeled the formation of up to 230 pg m^{-3} RGM in a regional model that does not include the reservoir of elevated RGM in the upper troposphere. If the elevated RGM in the upper troposphere predicted by Selin et al. had been included, this might have resulted in higher RGM in the model used here.

[68] A critical issue pertaining to the chemistry of mercury is the mechanism for reduction of RGM to Hg^0 . As noted in section 3 the reduction of RGM through aqueous reactions with HO_2 and O_2^- has been included here, although the viability of these reactions was challenged by Gardfeldt and Jonsson [2003]. Model results with this reaction omitted are shown in Figure 14.

[69] The aqueous reduction of RGM apparently has little effect on the highest ambient RGM, which result from

extended cloud-free periods. However, the omission of the aqueous reduction results in significantly higher RGM at times and locations with relatively low or moderate concentrations. This impact is largest near the surface, where air may be processed more frequently by nonprecipitating clouds or fog. Average ambient RGM is increased by 50% near the surface and by 20% at 1.3–3.7 km in the simulation without the aqueous reduction reactions. Because of the large effect at ground level the reduction reactions may affect assessments of the relative importance of dry versus wet deposition as a source of mercury.

[70] The changes in RGM in the model with the aqueous reduction reactions are episodic and are associated with nonprecipitating clouds and fog. The episodic nature is illustrated in the diurnal profile (Figure 15). Ambient RGM is similar in models with and without the aqueous reactions during the daytime, but at night RGM decreases sharply only when the aqueous reactions are included. For the comparison with measured RGM (see Figure 5b) the change in model chemistry causes a significant increase in RGM at only two locations corresponding to measurements. These changes would cause the model to overestimate RGM by a factor of two at lower altitudes (400–1700 m) that correspond to the lowest measured RGM. Little change was found at higher altitudes or in places with the highest ambient RGM.

[71] Figure 14 also shows the results of model calculations with all aqueous reactions removed. The results with no aqueous chemistry are similar to results without the reduction reaction. RGM is increased by an additional 10% near the surface at 5% at 1.3–3.7 km in comparison with the simulation without the aqueous reduction of RGM but with all other aqueous reactions included. This suggests that the other aqueous reactions have relatively little impact on RGM. However, the similarity between the results with no aqueous chemistry and the results with only the reduction reaction removed may be due to compensating factors. Removal of the aqueous reactions results in higher gas phase OH and leads to faster production of RGM. This

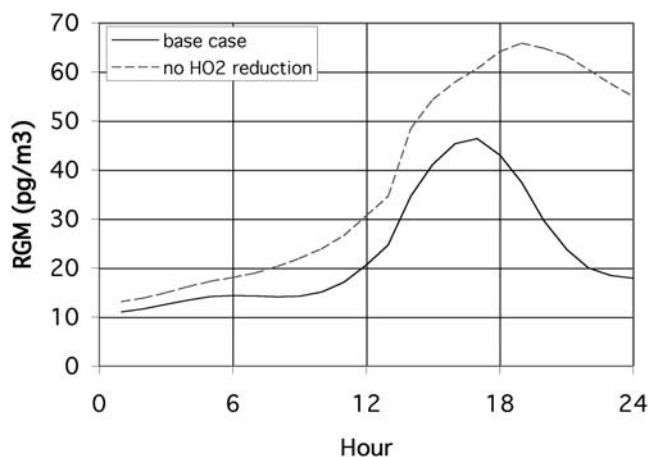


Figure 15. Diurnal profiles for RGM on 12 June at 0–0.2 km altitude, 25.9°N, 80.2°W (just west of Miami), in (a) the original simulation (solid line) and (b) a simulation with the aqueous reaction of RGM with HO_2 and O_2^- removed (dashed line).

compensates for the omission of reactions that produce aqueous RGM in the simulation without aqueous chemistry.

[72] *Shia et al.* [1999] reported that omission of aqueous reactions in a global model causes a 25% decrease in total atmospheric mercury. This is broadly consistent with our findings in that both *Shia et al.* and this work report an increase in the ratio RGM/Hg⁰ when aqueous chemistry is omitted. Here, Hg⁰ was determined mainly by initial and boundary conditions, so that removal of aqueous reactions affects RGM and the RGM/Hg⁰ ratio but has little effect on Hg⁰. Hg⁰ was determined by global balances in the model reported by *Shia et al.*, and removal of aqueous reactions resulted in lower Hg⁰ rather than increased RGM (which accounts for most of the removal of atmospheric mercury).

6. Conclusions

[73] We have described a regional-scale model for the photochemistry and transport of speciated mercury, including a fully integrated solution for gas phase and aqueous chemistry and photochemical reactions for O₃, OH, NO_x, organics, sulfur, halogens, mercury and related species.

[74] The model results describe a process in which RGM is formed slowly through gas phase reactions and removed rapidly by aqueous reduction in clouds. Results show that intermittent high RGM (up to 260 pg m⁻³) forms over the Atlantic Ocean, with elevated RGM occurring in air with a cloud-free history. Measurements in south Florida found RGM varying between 10 and 230 pg m⁻³ and increasing with height, a pattern that was largely reproduced by the model. Although the model underpredicted the maximum RGM by a factor of two in site-by-site comparison with measurements, the model generated high RGM over the Atlantic Ocean near Florida with magnitudes comparable to the measured Florida maximum. The intermittent high RGM in the model in combination with the high observed RGM in Florida, suggest that elevated RGM can be produced by photochemical processes. Model results for RGM may also be interpreted as confirmation of the proposed reaction of Hg⁰ with OH, because elevated RGM in the model is dependent on this reaction.

[75] The aqueous chemistry of mercury in the model is strongly affected by the uncertain reaction of RGM with HO₂ and O₂⁻, proposed by *Pehkonen and Lin* [1998] and challenged by *Gardfeldt and Jonsson* [2003]. When this reaction is removed from the mechanism ambient RGM at the surface increases by 50%, although the maximum RGM does not change much. The remaining aqueous reactions have relatively little net effect on RGM in the simulation.

[76] The model described here contains significant uncertainty as a predictor of source-receptor relationships for atmospheric mercury. Direct emission rates and rates of the reactions that convert Hg⁰ to RGM and vice versa are uncertain, formation of particulate mercury has been omitted, and the coarse resolution of the model shown here may compromise its ability to identify the impact of local sources. For this reason the proposed measurement-based tests for the accuracy of model source-receptor relationships assume a special importance. The results are also limited by the size of the model domain, the short duration and spin-up time, and the omission of soil recycling. Results are also sensitive to Hg⁰ at the model boundary.

[77] Model results show an anticorrelation between RGM and Hg⁰ in regions where RGM is formed primarily by photochemical production and a positive correlation between RGM and Hg⁰ in regions where RGM originates primarily from direct emissions. This predicted correlation may provide a basis for evaluating the accuracy of model sensitivity predictions for RGM by comparing with measured correlations. If measured correlations between Hg⁰ and RGM are consistent with model results, it will provide a level of validation for the model sensitivity predictions. By contrast, if measured correlations differ from model results, it will suggest that the model sensitivity predictions are also suspect. Correlations between RGM and either SO₂ or NO_y are also predicted for directly emitted RGM, and correlations between RGM and H₂O₂ are predicted for photochemically produced RGM.

[78] The model also predicts that ambient RGM is increased by up to 50% during pollution events in the eastern United States with elevated O₃, resulting from the same photochemistry that produces O₃. Because formation of RGM is relatively slow, the enhanced RGM is likely to occur only during events with persistent elevated O₃ extending over a wide region. A strong correlation is predicted between RGM and O₃ in these situations. Future work will explore whether this predicted correlation can be confirmed by ambient measurements.

[79] The predicted high RGM over the Atlantic Ocean and its spatial variation are both strongly affected by the distribution of clouds. The distribution of RGM therefore depends critically on the accuracy of the representation of clouds in regional and global models and may be especially sensitive to representations of clouds with small spatial extent. It is noteworthy that model RGM is generally higher over the Atlantic Ocean and Caribbean than in the eastern United States. Measured wet deposition of Hg in the United States tends to be highest in Florida and along the coast of the Gulf of Mexico, although direct emissions are higher in the northeast and midwest. If the meteorology during these events is representative, then the distribution of ambient RGM associated with photochemical conversion from Hg⁰ may partly explain the high wet deposition in the southeastern United States. *Selin et al.* [2007] and *Seigneur et al.* [2004] also found that the high wet deposition in the eastern United States was due to meteorology.

[80] Some additional activity is needed to complete the results shown here. This includes extension of the model to include representation of particulate mercury; a comparison with results of other versions of CMAQ to establish the impact of the integrated gas/aqueous solver, and evaluation of the predicted correlation between RGM and O₃ in comparison with measurements.

Appendix A: Numerical Solution for Gas and Aqueous Phase Photochemistry

[81] The solution for photochemistry is based on the implicit (reverse Euler) equations but incorporates a number of nonstandard treatments described by *Sillman* [1991] and *Barth et al.* [2003].

[82] The iterative Newton Raphson solution to the implicit equations is time-consuming because each iteration requires the inversion of a large matrix. Its use in atmo-

spheric models is often based on sparse matrix inversion methods. Here, the solution for gas phase species is done by solving the implicit equations for individual species or for pairs of closely interacting species in sequential order from reactants to products. OH and HO₂ are then solved for on the basis of an equation for summed production and loss of odd hydrogen radicals, as described by *Sillman* [1991].

[83] The procedure for aqueous chemistry involves a sequential iterative calculation with two stages: (1) calculation of gas-aqueous partitioning and aqueous dissociation (based on Henry's law and equilibrium constants, and including calculation of [H⁺] and [OH⁻]), and (2) calculation of changes in species concentrations due to photochemical production and loss. The calculation of species concentrations is based on photochemical production and loss for a sum of species related by Henry's law and aqueous dissociation and equilibria (e.g., H₂SO₄(g), H₂SO₄(a), HSO₄⁻ and SO₄²⁻), while the partitioning among these species is left unchanged.

[84] Mathematically, this is the equivalent of a reverse Euler solution with inversion of a sparse matrix, in which it is assumed that certain matrix elements are approximated as zero. The reverse Euler iterative solution, using Newton Raphson procedure, is:

$$c_i^{t+\Delta t} = c_i^P + \left(I - \frac{\partial R_i^P}{\partial c_j} \right)^{-1} (c_j^t + R_j^P - c_j^P) \quad (\text{A1})$$

where c_i^t represents the matrix of species concentrations at time t , c_i^P represents the estimate for $c_i^{t+\Delta t}$ from the prior iteration, I represents the identity matrix and R_j^P represents the rate of photochemical production and loss during the interval Δt , calculated on the basis of c_i^P . The procedure effectively decomposes the concentration matrix into terms representing the sum of gas, aqueous and disassociated species, and terms for individual species derived from the partitioning of the sum. The Jacobian terms dR_i/dc_j are assumed to be zero for the R_i terms representing gas-aqueous partitioning with c_j for species not directly linked through Henry's law or equilibrium constants. This assumption allows gas-aqueous partitioning to be calculated separately, rather than included in the inversion of the large Jacobian matrix.

[85] Partitioning between gas and aqueous species is based on Henry's law exchange coefficients, rates of gas-to-aqueous transfer, and first-order photochemical removal rates for the individual gas and aqueous species (including aqueous species that are linked through dissociation, which is assumed to occur instantaneously). Values of H⁺ and OH⁻ from the previous iteration are used to establish partitioning based on aquatic equilibria. The gas-aqueous transfer rate is derived as described by *Lelieveld and Crutzen* [1991]. Photochemical production and loss terms are from the previous iteration. The resulting equation for gas-aqueous partition is given by (2) in section 2.1. In addition, an adjustment to the Henry's law constant is made to account for situations in which aqueous phase diffusion is a limiting factor for aqueous chemistry, using methods described by *Lelieveld and Crutzen* [1991].

[86] The aqueous-gas concentration ratio, aquatic equilibrium constants and values of H⁺ and OH⁻ from the previous iteration are used to establish partitioning among

linked gas and aqueous species, while the sum of gas and linked aqueous species is kept unchanged. Following the aqueous partitioning, H⁺ and OH⁻ are calculated from the ionic balance. This calculation results in a convergent solution only if the impact of H⁺ and OH⁻ on the partitioning of aqueous equilibria is included. This is done using reverse Euler format, as follows:

$$c_h^{t+\Delta t} = c_h^P + \frac{\sum_i n_i c_i}{1 - \sum_i \partial(n_i c_i) / \partial c_h^P} \quad (\text{A2})$$

where c_h^P represents the prior concentration of H⁺ and $\sum n_i c_i$ represents the summed charge among aqueous species (concentrations c_i weighted by negative charge n_i). The sum $\partial(n_i c_i) / \partial c_h^P$ represents the sensitivity of charged aqueous concentrations to H⁺, based on the aquatic equilibria and prior H⁺. This solution is also equivalent to the a reverse Euler solution in which it is assumed that all terms of the Jacobian matrix relating to H⁺ are zero, except those relating to the partitioning of aqueous species.

[87] After gas-aqueous partitioning and H⁺ have been established, the final stage of the iterative procedure is the calculation of species calculations based on photochemical production and loss. This is done as by *Sillman* [1991], using equations that represent summed concentrations of gas and aqueous species that are linked through Henry's law and aquatic equilibrium constants. The solution also uses the reverse-Euler equation (1) along with the assumption that many of the terms of the Jacobian matrix are zero. Equation (1) is used sequentially to calculate concentrations for individual species (or for two closely linked species, such as NO₃ and N₂O₅), with specified order, from reactants to products. A separate solution is provided for the odd hydrogen radicals, OH and HO₂, based on radical sources and sinks. Much of the complexity of the stiff system (including the complex dependence of radical sources and sinks on OH and HO₂) is represented in the solution for odd hydrogen. The result is a convergent solution to the complete reverse-Euler equation (1) without a direct inversion of the Jacobian matrix. When aqueous chemistry is included the solution for OH and HO₂ is expanded to include HCO₃ and CO₃²⁻, which rapidly interchange with aqueous OH, HO₂ and O₂⁻.

[88] Implicit methods of this type are computationally advantageous because they provide convergent solutions for photochemical evolution long time intervals. The time interval for the iterative solution (here, 30 min) might lead to numerical errors in representing air parcels that are intermittently exposed to clouds on shorter timescales. However, *Barth et al.* [2003] reported that there is little difference in photochemical evolution based on exposure to clouds for 10-min intervals as opposed to 30-min intervals, assuming the same total exposure to cloud. As reported by *Barth et al.*, there is also no significant difference in test results for this procedure based on 5-min versus 30-min time steps.

[89] **Acknowledgments.** The United States Environmental Protection Agency through its Office of Research and Development and National Center for Environmental Research funded this work under STAR grant EPA R-82979901-0. It has been subject to Agency Review and approved for publication. Mention of trade names or commercial products does not

constitute an endorsement or recommendation for use. Additional support was provided by the National Science Foundation grant 0454838. Any opinions, findings, and conclusions or recommendations expressed in this material are those of the authors and do not necessarily reflect the views of the National Science Foundation. Meteorological data were provided by the Data Support Section of the Computational and Information Systems Laboratory at the National Center for Atmospheric Research. NCAR is supported by grants from the National Science Foundation. We thank the NOAA Flight Operations Center and Atmospheric Research Laboratory staff for support during aircraft operations, particularly pilot Jeff Hagan (FOC) and Winston Luke (ARL).

References

- Ariya, P. A., A. Khalizov, and A. Gidas (2002), Reactions of gaseous mercury with atomic and molecular halogens: Kinetics, product studies, and atmospheric implications, *J. Phys. Chem. A*, *106*(32), 7310–7320.
- Barth, M., S. Sillman, R. Hudman, M. Z. Jacobson, C.-H. Kim, A. Monod, and J. Liang (2003), Summary of the cloud chemistry modeling intercomparison: Photochemical box model calculation, *J. Geophys. Res.*, *108*(D7), 4214, doi:10.1029/2002JD002673.
- Bash, J. O., D. R. Miller, T. H. Meyer, and P. A. Bresnahan (2004), Northeast United States and southeast Canada natural mercury emissions estimated with a surface emission model, *Atmos. Environ.*, *38*, 5683–5692.
- Bullock, O. R., and K. A. Brehme (2002), Atmospheric mercury simulation using the CMAQ model: formulation description and analysis of wet deposition results, *Atmos. Environ.*, *36*(13), 2135–2146.
- Byun, D., and K. L. Schere (2006), Review of the governing equations, computational algorithms, and other components of the Models-3 Community Multiscale Air Quality (CMAQ) modeling system, *Appl. Mech. Rev.*, *59*, 51–77.
- Calvert, J. G., and S. E. Lindberg (2003), A modeling study of the mechanism of the halogen-ozone-mercury homogeneous reactions in the troposphere during the polar spring, *Atmos. Environ.*, *37*(32), 4467–4481.
- Calvert, J. G., and S. E. Lindberg (2004), The potential influence of iodine-containing compounds on the chemistry of the troposphere in the polar spring. II. Mercury depletion, *Atmos. Environ.*, *38*(30), 5105–5116.
- Dastoor, A. P., and Y. Laroque (2004), Global circulation of atmospheric mercury: A modeling study, *Atmos. Environ.*, *38*, 147–161.
- Deguillaume, L., M. Leriche, A. Monod, and N. Chaumerliac (2003), The role of transition metal ions on HOx radicals in clouds: A numerical evaluation of its impact on multiphase chemistry, *Atmos. Chem. Phys. Disc.*, *3*, 5019–5060.
- Evans, M. J., A. Fiore, and D. J. Jacob (2003), The GEOS-CHEM chemical mechanism version 5-07-8, Harvard Univ., Cambridge, Mass. (Available at http://www.env.leeds.ac.uk/~mat/GEOS-CHEM/geoschem_mech.pdf)
- Feng, Y., J. E. Penner, S. Sillman, and X. Liu (2004), Effects of cloud overlap in photochemical models, *J. Geophys. Res.*, *109*, D04310, doi:10.1029/2003JD004040.
- Gardfeldt, K., and M. Jonsson (2003), Is bimolecular reduction of Hg (II) complexes possible in aqueous systems of environmental importance, *J. Phys. Chem. A*, *107*(22), 4478–4482.
- Gardfeldt, K., J. Sommar, D. Stromberg, and X. Feng (2001), Oxidation of atomic mercury by hydroxyl radicals and photoinduced decomposition of methylmercury in the aqueous phase, *Atmos. Environ.*, *35*, 3039–3047.
- Gbor, P. K., D. Wen, F. Meng, F. Yang, B. Zhang, and J. J. Sloan (2006), Improved model for mercury emission, transport and deposition, *Atmos. Environ.*, *40*(5), 973–983.
- Gbor, P. K., D. Wen, F. Meng, F. Yang, B. Zhang, and J. J. Sloan (2007), Modeling of mercury emission, transport and deposition in North America, *Atmos. Environ.*, *41*(6), 1135–1149.
- Grell, G. A., J. Dudhia, and D. R. Stauffer (1994), A description of the fifth-generation Penn State/NCAR mesoscale model (MM5), *NCAR Tech. Note, NCAR/TN-398+STR*, 117 pp., Natl. Cent. for Atmos. Res., Boulder, Colo.
- Hall, B. (1995), The gas-phase oxidation of elemental mercury by ozone, *Water Air Soil Pollut.*, *80*, 301–315.
- Hedgecock, I. M., G. A. Trunfio, N. Pirrone, and F. Sprovieri (2005), Mercury chemistry in the MBL: Mediterranean case and sensitivity studies using the AMCOTS (Atmospheric Mercury Chemistry over the Sea) model, *Atmos. Environ.*, *39*(38), 7217–7230.
- Hedgecock, I. M., N. Pirrone, G. A. Trunfio, and F. Sprovieri (2006), Integrated mercury cycling, transport, and air-water exchange (MECAWEX) model, *J. Geophys. Res.*, *111*, D20302, doi:10.1029/2006JD007117.
- Irshad, H., A. R. McFarland, M. S. Landis, and R. K. Stevens (2004), Wind tunnel evaluation of an aircraft-borne sampling system, *Aerosol Sci. Technol.*, *38*, 311–321.
- Ito, A., S. Sillman, and J. E. Penner (2007), Effects of additional non-methane volatile organic compounds, organic nitrates, and direct emissions of oxidized organic species on global tropospheric chemistry, *J. Geophys. Res.*, *112*, D06309, doi:10.1029/2005JD006556.
- Jacob, D. J. (1986), Chemistry of OH in remote clouds and its role in the production of formic acid and peroxymonosulfate, *J. Geophys. Res.*, *91*, 9807–9826.
- Jacob, D. J. (2000), Heterogeneous chemistry and tropospheric ozone, *Atmos. Environ.*, *34*(12–14), 2131–2159.
- Khalizov, A. F., B. Viswanathan, P. Larregaray, and P. A. Ariya (2003), A theoretical study on the reactions of Hg with halogens: Atmospheric implications, *J. Phys. Chem. A*, *107*(33), 6360–6365.
- Landis, M. S., R. K. Stevens, F. Schaedlich, and E. Prestbo (2002), Development and characterization of an annular denuder methodology for the measurement of divalent inorganic reactive gaseous mercury in ambient air, *Environ. Sci. Technol.*, *36*, 3000–3009.
- Landis, M. S., M. Lynam, and R. K. Stevens (2005), The monitoring and modeling of mercury species in support of local regional and global modeling, in *Dynamics of Mercury Pollution on Regional and Global Scales*, edited by N. Pirrone and K. R. Mahaffey, pp. 123–151, Kluwer Acad., New York.
- Lelieveld, J., and P. J. Crutzen (1990), Influences of cloud photochemical processes on tropospheric ozone, *Nature*, *343*, 227–233.
- Lelieveld, J., and P. J. Crutzen (1991), The role of clouds in tropospheric photochemistry, *J. Atmos. Chem.*, *12*, 229–267.
- Lin, C.-J., and S. O. Pehkonen (1998a), Two-phase model of mercury chemistry in the atmosphere, *Atmos. Environ.*, *32*(14/15), 2543–2558.
- Lin, C.-J., and S. O. Pehkonen (1998b), Oxidation of elemental mercury by aqueous chlorine (HOCl/OCl⁻): Implications for troposphere mercury chemistry, *J. Geophys. Res.*, *103*(D21), 28,093–28,102.
- Lin, C.-J., and S. O. Pehkonen (1999), The chemistry of atmospheric mercury: A review, *Atmos. Environ.*, *33*, 2067–2079.
- Lin, C.-J., S. E. Lindberg, T. C. Ho, and C. Jang (2005), Development of a processor in BEIS3 for estimating vegetative mercury emission in the continental United States, *Atmos. Environ.*, *39*, 7529–7540.
- Lin, C.-J., P. Pongprueks, S. E. Lindberg, S. O. Pehkonen, D. Byun, and C. Jang (2006), Scientific uncertainties in atmospheric mercury models I: Model science evaluation, *Atmos. Environ.*, *40*, 2911–2928.
- Lin, X., and Y. Tao (2003), A numerical modelling study on regional mercury budget for eastern North America, *Atmos. Chem. Phys.*, *3*, 535–548.
- Lindberg, S. E., S. Brooks, C.-J. Lin, K. J. Scott, M. S. Landis, R. K. Stevens, M. Goodsite, and A. Richter (2002a), Dynamic oxidation of gaseous mercury in the Arctic troposphere at polar sunrise, *Environ. Sci. Technol.*, *36*, 1245–1256.
- Lindberg, S. E., W. Dong, and T. Meyers (2002b), Transpiration of gaseous elemental mercury through vegetation in a subtropical wetland in Florida, *Atmos. Environ.*, *36*, 5207–5219.
- Liu, X., G. Mauersberger, and D. Moeller (1997), The effects of cloud processes on the tropospheric photochemistry: An improvement of the EURAD model with a coupled gaseous and aqueous chemical mechanism, *Atmos. Environ.*, *31*, 3119–3135.
- Logan, J. A. (1999), An analysis of ozonesonde data for the troposphere: Recommendations for testing 3-D models and development of a gridded climatology for tropospheric ozone, *J. Geophys. Res.*, *104*, 16,115–16,149.
- Madronich, S., and S. Flocke (1998), The role of solar radiation in atmospheric chemistry, in *Handbook of Environmental Chemistry*, edited by P. Boule, pp. 1–16, Springer, New York.
- Malcolm, E. G., G. J. Keeler, and M. S. Landis (2003), The effects of the coastal environment on the atmospheric mercury cycle, *J. Geophys. Res.*, *108*(D12), 4357, doi:10.1029/2002JD003084.
- Mao, H., and R. Talbot (2004), Role of meteorological processes in two New England ozone episodes during summer 2001, *J. Geophys. Res.*, *109*, D20305, doi:10.1029/2004JD004850.
- Mebust, M. R., B. K. Eder, F. S. Binkowski, and S. J. Roselle (2003), Models-3 Community Multiscale Air Quality (CMAQ) model aerosol component: 2. Model evaluation, *J. Geophys. Res.*, *108*(D6), 4184, doi:10.1029/2001JD001410.
- Monod, A., and P. Carlier (1999), Impact of clouds on the tropospheric ozone budget: Direct effect of multiphase photochemistry of soluble organic compounds, *Atmos. Environ.*, *33*(27), 4431–4446.
- Olson, J., et al. (1997), Results from the Intergovernmental Panel on Climatic Change Photochemical Model Intercomparison (PhotoComp), *J. Geophys. Res.*, *102*, 5979–5991.
- Pai, P., P. Karamchandani, and C. Seigneur (1997), Simulation of the regional atmospheric transport and fate of mercury using a comprehensive Eulerian model, *Atmos. Environ.*, *31*(17), 2717–2732.
- Pal, B., and P. A. Ariya (2004), Studies of ozone initiated reactions of gaseous mercury: Kinetics, product studies and atmospheric implications, *Phys. Chem. Chem. Phys.*, *6*, 572–579.

- Pandis, S. N., and J. H. Seinfeld (1989), Sensitivity analysis of a chemical mechanism for aqueous-phase atmospheric chemistry, *J. Geophys. Res.*, *94*, 1105–1126.
- Pehkonen, S. O., and C.-J. Lin (1998), Aqueous photochemistry of divalent mercury with organic acids, *J. Air Waste Manage. Assoc.*, *48*, 144–150.
- Petersen, G., R. Bloxam, S. Wong, J. Munthe, O. Krüger, S. Schmolke, and V. A. Kumar (2001), A comprehensive Eulerian modeling framework for airborne species: Model development and applications in Europe, *Atmos. Environ.*, *35*, 3063–3074.
- Pleijel, K., and J. Munthe (1995), Modeling the atmospheric mercury cycle-chemistry in fog droplets, *Atmos. Environ.*, *29*(12), 1441–1457.
- Pruppacher, H. R., and J. D. Klett (1997), *Microphysics of Clouds and Precipitation*, Kluwer Acad., Dordrecht, Netherlands.
- Ryaboshapko, A., R. Bullock, R. Ebinghaus, I. Ilyin, K. Lohman, J. Munthe, G. Petersen, C. Seigneur, and I. Wängberg (2002), Comparison of mercury chemistry models, *Atmos. Environ.*, *36*(24), 3881–3898.
- Ryerson, T. B., et al. (1998), Emissions lifetimes and ozone formation in power plant plumes, *J. Geophys. Res.*, *103*, 22,569–22,584.
- Sander, R., and P. J. Crutzen (1996), Model study indicating halogen activation and ozone destruction in polluted air masses transported to the sea, *J. Geophys. Res.*, *101*, 9121–9138.
- Sander, R., et al. (2003), Inorganic bromine in the marine boundary layer: A critical review, *Atmos. Chem. Phys. Disc.*, *3*, 2963–3050.
- Schroeder, W. H., and J. Munthe (1998), Atmospheric mercury—An overview, *Atmos. Environ.*, *32*, 809–822.
- Schwartz, S. E. (1986), Mass-transport considerations pertinent to aqueous-phase reactions of gases in liquid-water clouds, in *Chemistry of Multi-phase Atmospheric Systems*, vol. G6, edited by W. Jaeschke, pp. 415–471, Springer, New York.
- Seigneur, C., K. Vijayaraghavan, K. Lohman, P. Karamchandani, and C. Scott (2004), Global source attribution for mercury deposition in the United States, *Environ. Sci. Technol.*, *38*(2), 555–569.
- Selin, N. E., D. J. Jacob, R. J. Park, R. M. Yantosca, S. Strode, L. Jaegle, and D. Jaffe (2007), Chemical cycling and deposition of atmospheric mercury: Global constraints from observations, *J. Geophys. Res.*, *112*, D02308, doi:10.1029/2006JD007450.
- Shia, R.-L., C. Seigneur, P. Pai, M. Ko, and N. D. Sze (1999), Global simulation of atmospheric mercury concentrations and deposition fluxes, *J. Geophys. Res.*, *104*(D19), 23,747–23,760.
- Sillman, S. (1991), A numerical solution to the equations of tropospheric chemistry based on an analysis of sources and sinks of odd hydrogen, *J. Geophys. Res.*, *96*, 20,735–20,744.
- Sommar, J., K. Gardfeldt, D. Stromberg, and X. Feng (2001), A kinetic study of the gas-phase reaction between the hydroxyl radical and atomic mercury, *Atmos. Environ.*, *35*, 3049–3054.
- Spivakovsky, C. M., et al. (2000), Three-dimensional climatological distribution of tropospheric OH: Update and evaluation, *J. Geophys. Res.*, *105*, 8931–8980.
- Sumner, A. L., C. W. Spicer, J. Satola, R. Mangaraj, C. A. Cowen, M. S. Landis, R. K. Stevens, and T. D. Atkeson (2005), Environmental chamber studies of mercury reactions in the atmosphere, in *Dynamics of Mercury Pollution on Regional and Global Scales*, edited by N. Pirrone and K. R. Mahaffey, pp. 193–212, Kluwer Acad., New York.
- Swartzendruber, P. C., D. A. Jaffe, E. M. Prestbo, P. Weiss-Penzias, N. E. Selin, R. Park, D. J. Jacob, S. Strode, and L. Jaegle (2006), Observations of reactive gaseous mercury in the free troposphere at the Mount Bachelor Observatory, *J. Geophys. Res.*, *111*, D24301, doi:10.1029/2006JD007415.
- U.S. Environmental Protection Agency (1997a), An inventory of anthropogenic mercury emissions in the United States, *Mercury Study Report to Congress*, vol. III, EPA-452/R-97-004, U.S. Govt. Print. Off., Washington, D. C. (Available at <http://www.epa.gov/ttn/chief/net/1999inventory.html#final3haps>)
- U.S. Environmental Protection Agency (1997b), Fate and transport of mercury in the environment, *Mercury Study Report to Congress*, vol. III, EPA-452/R-97-005, U.S. Govt. Print. Off., Washington, D. C.
- U.S. Environmental Protection Agency (2004), 1999 National Emission Inventory Documentation and Data—Final Version 3.0, Research Triangle Park, N. C. (Available at <http://www.epa.gov/ttn/chief/net/1999inventory.html#final3crit>)
- van Loon, L., E. Mader, and S. Scott (2000), Reduction of the aqueous mercuric ion by sulfite: UV spectrum of HgSO₃ and its intramolecular redox reaction, *J. Phys. Chem.*, *104*, 1621–1626.
- Walcek, C. J., and G. R. Taylor (1986), A theoretical method for computing vertical distributions of acidity and sulfate production within cumulus clouds, *J. Atmos. Sci.*, *43*, 339–355.
- Weinstein-Lloyd, J. B., J. H. Lee, P. H. Daum, L. I. Kleinman, L. J. Nunnermacker, S. R. Springston, and L. Newman (1998), Measurements of peroxides and related species during the 1995 summer intensive of the Southern Oxidants Study in Nashville, Tennessee, *J. Geophys. Res.*, *103*(D17), 22,361–22,374.
- Weiss-Penzias, P., D. A. Jaffe, A. McClintick, E. Prestbo, and M. S. Landis (2003), Gaseous elemental mercury in the marine boundary layer: Evidence for rapid removal in anthropogenic pollution, *Environ. Sci. Technol.*, *37*, 3755–3763.
- Xu, X., X. Yang, D. R. Miller, J. J. Helble, and R. J. Carley (2000a), A regional scale modeling study of atmospheric transport and transformation of mercury. I. Model development and evaluation, *Atmos. Environ.*, *34*, 4933–4944.
- Xu, X., X. Yang, D. R. Miller, J. J. Helble, and R. J. Carley (2000b), A regional scale modeling study of atmospheric transport and transformation of mercury. II. Simulation results, *Atmos. Environ.*, *34*, 4945–4955.

K. I. Al-Wali, G. J. Keeler, F. J. Marsik, and S. Sillman, Department of Atmospheric, Oceanic and Space Sciences, University of Michigan, Ann Arbor, MI 48109-2143, USA. (sillman@umich.edu)

M. S. Landis, Office of Research and Development, U.S. Environmental Protection Agency, Research Triangle Park, NC 27711, USA.